Loss of PAX6 alters the excitatory/inhibitory neuronal ratio in human cerebral organoids.

Wai Kit Chan[1], Shibla Abdulla[1], Lusi Zhao[1], Danilo Negro[1], Victoria M. Munro[1], Helen Marshall[1], Zrinko Kozić[1], Megan Brown[1], Michela Barbato[1], Mariana Beltran[2], Neil C Henderson[2], David J. Price[1], John O. Mason[1]

[1]Simons Initiative for the Developing Brain, Institute for Neuroscience and Cardiovascular Research, University of Edinburgh, Hugh Robson Building, George Square, Edinburgh EH8 9XD, UK

[2]Institute for Regeneration & Repair (IRR), University of Edinburgh, Edinburgh Bioquarter, 4 – 7 Little France Drive, Edinburgh EH16 4UU, United Kingdom.

Corresponding Author email address: waikit.chan@ed.ac.uk

Keywords: PAX6, human cerebral organoid, neurodevelopment, cell fate, interneurons, cerebral cortex

Summary Statement (30 words)

Human cerebral organoids lacking PAX6 expression show an altered excitatory to inhibitory neuronal ratio, concomitant with altered responses to intercellular PTN-PTPRZ1 signalling.

Abstract (152/180 words)

The transcription factor PAX6 is a crucial regulator of multiple aspects of embryonic forebrain development. It has well-established roles in the regulation of excitatory and inhibitory neuron development in the embryonic cortex in mice but PAX6's roles during human forebrain development are less well understood. Using human cerebral organoids, we investigated PAX6's roles in human neurodevelopment. Homozygous PAX6 mutant (*PAX6*$^{-/-}$) organoids were larger than controls and contained increased inhibitory cell types. Excitatory neurons were still generated in *PAX6*$^{-/-}$ organoids but they were less mature, and a subset showed dysregulated expression of inhibitory identity genes compared to *PAX6*$^{+/+}$ controls. The inhibitory cells found in *PAX6*$^{-/-}$ organoids physically segregated from excitatory neurons and presented a distinct transcriptomic profile when compared to *in vivo* cortical inhibitory neurons. *PAX6*$^{-/-}$ organoids showed a dysregulated cellular response to PTN-PTPRZ1 signalling, which contributed to the observed increase in inhibitory neurons and the consequent altered excitatory to inhibitory neuronal ratio.

Introduction

Neurons in the cerebral cortex fall into two major classes – excitatory (which express the neurotransmitter glutamate) and inhibitory (which express the neurotransmitter GABA) (Cadwell et al., 2019). Excitatory neurons are born in the dorsal telencephalon while large numbers of inhibitory neurons are born ventrally, in the ganglionic eminences before migrating into the cortical plate to form cortical circuits with excitatory neurons. (Anderson et al., 1997; Anderson et al., 2001; Gorski et al., 2002) Recent evidence suggests that in humans, some cortical inhibitory neurons are born in the cortex alongside excitatory neurons (Chung et al., 2024; Delgado et al., 2022; Keefe et al., 2025; Wang et al., 2025a). Imbalances between these two cell types are thought to underlie a variety of neurodevelopmental disorders (Bruining et al., 2020). The transcription factor PAX6 is a key regulator of embryonic forebrain development playing a crucial role in cell fate determination (Manuel et al., 2015; Ochi et al., 2022; Walcher et al., 2013). In humans, homozygous PAX6 mutations are either lethal or result in major brain defects including corpus callosum agenesis, cortical thinning, microcephaly, large midline cavities and hypoplastic brainstem (Glaser et al., 1994; Schmidt-Sidor et al., 2009; Solomon et al., 2009). Human PAX6 is predominantly expressed in dorsal regions of the ventricular zone (VZ) in the telencephalon, the region that gives rise to excitatory neurons (Kerwin et al., 2010; Lindsay et al., 2005). Transcriptomic and *in situ* hybridisation analysis of the human fetal cortex revealed high *PAX6* expression in the anterior areas of the cortex that decreased caudally (Eze et al., 2021; Kerwin et al., 2010). In the dorsoventral axis, PAX6 is highly expressed dorsally with a decrease ventrally towards the ganglionic eminences forming a dorsoventral gradient of expression. Human PAX6 is expressed at low levels within the striatal subpallium, partly colocalizing with the ventral transcription factor OLIG2 (Kerwin et al., 2010; Mo and Zecevic, 2008). At more caudal levels however, the pallial/subpallial boundary (PSPB) is clearly delineated by a sharp border between the PAX6-expressing pallium located dorsally, which gives rise to glutamatergic neurons, and the OLIG2-expressing subpallium located ventrally from which GABAergic neurons arise (Kerwin et al., 2010). Besides the VZ, PAX6 is also expressed in the subventricular zone (SVZ) in human, including both the inner and outer subventricular zones (iSVZ and oSVZ) (Eze et al., 2021; Kerwin et al., 2010; Nowakowski et al., 2017; Pollen et al., 2015). The oSVZ is populated by outer radial glia (oRG) cells that characteristically marked by high expression

of PTPRZ1, a receptor for PTN (Hansen et al., 2010; Pollen et al., 2015; Reillo et al., 2011). However, the functional significance of PTN-PTPRZ1 signalling in oRGs during development is unknown. The expansion of oRGs, which express PAX6, is a key driver of cortical expansion and folding in human brain development due to their remarkable self-renewing capacity (Pollen et al., 2015). While the expression pattern of PAX6 in the developing human brain is reasonably well described, little is yet known about its functions in the developing human cortex. Studying cerebral organoids derived from *PAX6*$^{-/-}$ induced pluripotent stem cells (iPSCs), we found that PAX6 loss resulted in the generation of abnormal inhibitory cell types that segregate from other neuronal cell types and are transcriptomically abnormal. While excitatory neurons were still generated in the absence of functional PAX6, their maturation was delayed, and a subset of excitatory neurons were also transcriptionally abnormal. Thus, PAX6 loss resulted in organoids that have an altered excitatory to inhibitory ratio and we show that this was partially due to dysregulation of the PTN-PTPRZ1 signalling pathway.

Results

Generation of PAX6$^{-/-}$ *iPSCs and organoids*

PAX6 contains two DNA-binding domains, the paired box and homeodomain (Xu et al., 1999). Paired box mutations have been implicated in the brain malformations described in human patients (Tzoulaki et al., 2005) and the paired domain alone was found to be necessary and sufficient to regulate telencephalic development in mice (Haubst et al., 2004). Therefore, to study the role of PAX6 in human telencephalic development, we targeted the PAX6 loss of function mutation to the paired domain. We derived *PAX6*$^{-/-}$ mutant iPSC lines from the parental line NAS2 (Devine et al., 2011) using CRISPR-Cas9 to insert a T residue into the paired box region of PAX6 (Fig 1A), causing a frameshift mutation that results in premature termination of PAX6 protein at amino acid residue 31, 20 residues downstream of the mutation. Two independent *PAX6*$^{-/-}$ clones (A10 and B2) homozygous for this mutation and two isogenic control clones (Nas2 and Cas92) were selected for further analysis. We confirmed that PAX6 mutagenesis was successful by PAX6 immunostaining with an antibody specific for the paired box domain (Engelkamp et al., 1999) and western blot. The former confirmed absence of PAX6 paired domain in mutant organoids and the latter showed truncated PAX6 protein (Fig 1C-D). All iPSC lines used in this study were subjected to whole genome

107 sequencing (WGS) analysis. No changes were detected at any of the five predicted most likely
108 CRISPR off-target sites. Probing further to ascertain whether the targeting procedure may
109 have introduced mutations that could have compromised the iPSC lines, we found that no
110 impactful mutations that would affect pluripotency or genomic integrity of the iPSCs
111 (Supplementary Fig 1). All lines expressed pluripotency markers NANOG, OCT3/4 and TRA-1-
112 60 (Supplementary Fig 2A)(Devine et al., 2011). Cerebral organoids were grown from *PAX6*$^{+/+}$
113 (control: NAS2 & CAS92) and *PAX6*$^{-/-}$ mutant (A10 & B2) cell lines using a version of the
114 Lancaster protocol (Lancaster et al., 2013) modified by the inclusion of dual SMAD inhibition
115 to enhance neural lineage differentiation (Chambers et al., 2009) and growth factors BDNF &
116 NT3 to support growth and survival of neurons (Birey et al., 2017)(Supplementary Fig 2B).
117
118 ***PAX6*$^{-/-}$ *organoids were larger than controls but contained fewer rosettes***
119 We characterised the cerebral organoids generated from the iPSCs. To characterise the
120 morphology of day 60 organoids grown from both *PAX6*$^{-/-}$ mutant lines and two isogenic
121 control lines, we cryosectioned and stained for SOX2 (to mark neural progenitors) and N-CAD
122 (to identify neuroepithelium) (Fig 1E,F). Staining patterns were consistent between organoids
123 of the same genotype. Although *PAX6*$^{-/-}$ organoids appeared larger than controls, they showed
124 a lower density of rosettes (radial arrangements of columnar epithelial cells with a central
125 lumen resembling a cross-section of the developing neural tube). Organoid size was
126 approximated by measuring the area of the widest cross-section of each organoid. The cross-
127 sectional area of *PAX6*$^{-/-}$ organoids was 18.09 $\pm$ 1.80 mm^2 compared to 11.55 $\pm$ 2.40 mm^2 in
128 controls (Fig 1G). The proportion of organoid tissue containing neural rosettes (demarcated
129 by SOX2 and N-CAD staining (Gomes et al., 2020)) was 1.4% $\pm$ 0.29% in *PAX6*$^{-/-}$ organoids and
130 12.68% $\pm$ 1.57% in controls (Fig 1H). This decrease was due to a dramatically lower density of
131 rosettes in *PAX6*$^{-/-}$ organoids (Fig 1I). While *PAX6*$^{-/-}$ organoids had lower neural rosette density,
132 the size of individual rosettes did not differ significantly between *PAX6*$^{-/-}$ organoids and
133 controls (Fig 1J-K). We previously reported that *Pax6*$^{-/-}$ mouse cortex showed an increase in
134 inhibitory cell types that formed ectopias in the developing mouse cortex. These inhibitory
135 cell types do not integrate into the cortical plate (Manuel et al., 2022). Therefore, we
136 hypothesise that the increase in overall organoid size coupled with a decrease in neural
137 rosette formation in *PAX6*$^{-/-}$ organoids was due to the emergence of ectopic inhibitory cell
138 types. As organoids lack an anato mical axis (Cederquist et al., 2019), we define ectopic

139 inhibitory cell types in organoids as inhibitory cell types whose distribution do not interleave
140 with excitatory neurons as is usually seen in healthy cerebral organoids (Osaki et al., 2024;
141 Sharf et al., 2022) but instead form separate territories in this study.
142
143 ***Altered cellular composition in PAX6$^{-/-}$ cerebral organoids.***
144 To characterise the cell types present in *PAX6$^{-/-}$* and control organoids, we performed single
145 cell RNA sequencing (scRNAseq) on four independent batches of organoids with each batch
146 containing organoids grown from each of the four iPSC lines (two mutants: A10 and B2, and
147 two controls: NAS2 and CAS92). Following quality control steps to remove ambient RNA, dead
148 cells, doublets and stressed cells regularly found in brain organoids (Vértesy et al., 2022),
149 40,461 cells were retained for downstream analysis. Cells were annotated using CellTypist
150 (Domínguez Conde et al., 2022) trained on a developing human fetal brain dataset (Braun et
151 al., 2023). Annotation discrepancies were cross-checked against other models trained on
152 human brain organoid data (He et al., 2024), other developing human fetal brain datasets
153 (Wang et al., 2025a) and resolved using cell type specific marker genes described in previous
154 studies (Bhaduri et al., 2020; Braun et al., 2023; He et al., 2024; Shi et al., 2021; Uzquiano et
155 al., 2022; Yu et al., 2021) (Fig 2A,B). Our dataset contained radial glial progenitors (RGP)
156 expressing marker genes including *GLI3*, *VIM* and *SLC1A3*; intermediate progenitor cells (IPC)
157 expressing *NHLH1*, *HES6*, *EOMES*; two clusters of excitatory neurons: excitatory neuron 1 (EN1)
158 expressing *NEUROD2, NEUROD6, SLC17A7* and excitatory neuron 2 (EN2) expressing marker
159 genes including *NRXN1*, *RBFOX3*; inhibitory neuron progenitors that express *DLX2*, *DLX6,*
160 *TOP2A* and inhibitory neurons that express *GAD1, SLC32A1,* and *DLX2* (Fig 2B, Supplementary
161 Table 1). There were also two clusters containing small numbers of cells (<410). One of these
162 (110 cells) was annotated as "unknown" as CellTypist was unable to reach agreement over the
163 different trained models and none of the marker genes pointed towards a clear cell type
164 (Supplementary Table 1). The other cluster (404 cells) was annotated as "mixed" because
165 CellTypist annotated them as a mixture of excitatory and inhibitory neurons depending on the
166 reference model. However, marker genes in that cluster included *DDIT4* and *HSP90AB1* which
167 are typically found in stressed cells in organoids (Supplementary Table 1) (Vértesy et al., 2022).
168 Both "mixed" and "unknown" clusters were found in both *PAX6$^{+/+}$* and *PAX6$^{-/-}$* organoids and
169 were excluded from further analysis.
170

171 There was a change in the proportion of cell types found in PAX6-null organoids compared to
172 controls (Fig 2C). The proportions of each cell type found in *PAX6*$^{+/+}$ organoids were: RGP 28.7
173 ± 3.7%; IPC, 6.7 ± 1.2%; EN1, 62.1 ± 4.9%; EN2 0.2% ± 0.01%; inhibitory neuron progenitors,
174 1.8 ± 0.3%; and inhibitory neurons 0.2% ± 0.1%.
175
176 In *PAX6*$^{-/-}$ organoids the proportions were: RGP 21.4 ± 3.1%; IPC, 2.3 ± 1.1%; EN1, 14.9 ± 3.5%;
177 EN2, 5.1 ± 1.4%; inhibitory neuron progenitors, 18.4 ± 0.3%; and inhibitory neurons 36.5% ±
178 6.4%. Thus, *PAX6*$^{-/-}$ organoids showed a ~25% decrease in RGPs and a ~66% decrease in IPCs
179 but a ~922% increase in inhibitory neuron progenitors compared to *PAX6*$^{+/+}$ organoids (Fig 2C-
180 E). There was also a ~76% decrease in the number of EN1 neurons in mutant organoids (Fig
181 3C-E, blue). Inhibitory neurons (Fig 2C-E, red) were almost exclusively found in PAX*6*$^{-/-}$
182 organoids (36.5%) compared to *PAX6*$^{+/+}$ controls (0.2%), a ~18150% increase in mutants.
183 Finally, an excitatory neuronal cluster EN2 that was also almost exclusively found in P*AX6*$^{-/-}$
184 organoids, constituted 5.1 ± 1.2% of cells in PAX6-null organoids compared to 0.2 ± 0.01% in
185 *PAX6*$^{+/+}$ control organoids (Fig 2C, EN2 - orange), a 2450% increase in mutants. Graphing the
186 relative proportions of cell-types found in each individual sample showed that the cellular
187 composition was relatively consistent within organoids of each genotype, as were the
188 differences between *PAX6*$^{-/-}$ organoids and controls (Fig 2E).
189
190 In summary, we found that loss of PAX6 caused a reduction in the proportion of neural
191 progenitors (RGP & IPC), a decrease in the proportion of excitatory neurons (EN1 & EN2) and
192 an increase in the proportion of inhibitory progenitors and neurons (Fig 2D). The generation
193 of inhibitory cell types at the expense of excitatory cell type suggests that PAX6 loss results in
194 cell fate diversification of neural progenitors from an excitatory to an inhibitory fate.
195
196 ***Inhibitory and excitatory cell types are physically segregated within PAX6*$^{-/-}$ *organoids.***
197 While the scRNAseq results confirmed that loss of PAX6 results in the increased in inhibitory
198 neurons, it did not address whether the inhibitory neurons were ectopic. To answer this
199 question, we examined the distribution of excitatory and inhibitory identity cells in *PAX6*$^{+/+}$
200 and *PAX6*$^{-/-}$ organoids. We immunostained cryosections of day 60 organoids for TBR2 (EOMES)
201 to label cortical IP cells which differentiate into excitatory neurons and DLX2 to identify
202 inhibitory cell precursors (Fig 3A). Sections throughout each individual organoid were sampled

203 and reconstructed to form 3D models (Fig 3A). Voxels in each reconstructed organoid were
204 assigned a value corresponding to their relative level of expression of TBR2 or DLX2, giving a
205 readout of dorsal versus ventral identity for cell clusters (Fig 3B, Supplementary Fig 3). We did
206 not observe any inhibitory territory staining in the *PAX6*$^{+/+}$ organoids and our analysis clearly
207 identified distinct, separate excitatory and inhibitory territories in each *PAX6*$^{-/-}$ organoid (Fig
208 3C). However, we did find some of these DLX2+ cells in the scRNAseq in the *PAX6*$^{+/+}$ control
209 organoids, albeit a very small number (328 cells). This most likely indicates that detection of
210 *DLX2* mRNA by scRNAseq is more sensitive than detection of DLX2 protein by
211 immunofluorescence. Further, as we employed a sampling method of each organoid to build
212 the 3D models, the small number of cells could be missed during sampling. Nevertheless, the
213 separation of excitatory/inhibitory territories supports our hypothesis that PAX6 loss results
214 in the emergence of ectopic inhibitory cell types. We next wondered whether PAX6 loss
215 diverts neural progenitors only to specific inhibitory cell types.
216
217 ***Inhibitory cell types in PAX6$^{-/-}$ organoids are likely abnormal***
218 To identify the specific subtype(s) of these ectopic inhibitory neurons that were generated in
219 the *PAX6*$^{-/-}$ organoids, we integrated our dataset with a scRNAseq dataset from fetal human
220 ventral telencephalon (Yu et al., 2021), where the majority of inhibitory neurons found in the
221 cortex are generated, to determine whether the inhibitory cells found in the *PAX6*$^{-/-}$ organoids
222 are equivalent to specific inhibitory subtypes found in the developing human brain (Fig 4A-B).
223 For this analysis we focussed on the inhibitory neurons in the *PAX6*$^{-/-}$ organoids as they formed
224 the vast majority of the inhibitory neurons in our dataset, 8704 cells compared to just 20 cells
225 in the *PAX6*$^{+/+}$ control organoids. Co-clustering of inhibitory cells found in *PAX6*$^{-/-}$ organoids
226 with a specific inhibitory subtype in the developing fetal brain would indicate transcriptomic
227 similarity between them. However, we found that the inhibitory neurons in *PAX6*$^{-/-}$ organoids
228 did not cluster with any specific subtype (Fig 4B). The failure of these cells to co-cluster with
229 specific known fetal brain inhibitory subtypes suggests that they represent an aberrant
230 population with a distinct transcriptomic profile, rather than mis-specified normal inhibitory
231 neuron subtypes.
232
233 To further explore the nature of *PAX6*$^{-/-}$ inhibitory cells in our *PAX6*$^{-/-}$ organoids, we conducted
234 differential gene expression (DGE) analysis between *PAX6*$^{-/-}$ organoid inhibitory cells and

235 inhibitory cells in the human ventral telencephalon reference dataset. This revealed a total of
236 6,933 differentially expressed genes (DEGs), 337 of which were downregulated in the *PAX6*$^{-/-}$
237 organoids compared to the reference dataset and 6,596 were upregulated (Supplementary
238 Data). Plotting the top 20 DEGs in a heatmap revealed that all 20 were upregulated in *PAX6*$^{-/-}$
239 inhibitory cells (Fig 4C). Some DEGs, including *AUTS2*, *CASK* and *MBD5* are known to be
240 involved in neuronal development while others encode cellular membrane proteins
241 implicated in cellular signalling or cell morphology (*NRXN3*, *CTNNA2*, *TUBB3*, *ATRNL1* and
242 *ENOX1*) (Fig 4C). To get a more holistic view of the differences between inhibitory cells in *PAX6*$^{-}$
243 $^{/-}$ organoids and those in the developing fetal brain, we performed gene ontology (GO) analysis
244 on all 6933 DEGs. Top-ranked GO terms related to intra- and intercellular processes including
245 transcription, phosphorylation and intracellular signal transduction (Fig 4D). Looking at the
246 molecular function GO terms of the DEGs (Fig 4E), the main differences between inhibitory
247 neurons generated from the loss of PAX6 and *in vivo* developing inhibitory neurons are
248 dysregulated expression of genes involved in molecular interactions highlighted by most GO
249 terms being involved in the binding of molecules.
250
251 Taken together, the DGE between *PAX6*$^{-/-}$ inhibitory neurons and in vivo inhibitory neurons
252 suggests that the loss of PAX6 results in inhibitory neurons with defects in basic cellular
253 processes including disrupted transcriptional regulation, cell signalling and molecular binding.
254 The failure of *PAX6*$^{-/-}$ inhibitory neurons to establish proper molecular machinery for normal
255 function suggests that the inhibitory neurons that were born due PAX6 loss were abnormal
256 inhibitory neurons. Perhaps this might explain the extreme segregation into different
257 "territories" as we have described above that usually happens to abnormal cell types (Fig 3).
258
259 ***Excitatory cell types in PAX6*$^{-/-}$ *organoids are more immature than those in PAX6*$^{+/+}$ *controls.***
260 While inhibitory neurons numbers were increased in the expense of excitatory neurons in
261 *PAX6*$^{-/-}$ organoids, the organoids still contained a significant number of excitatory neurons (Fig
262 3C-E). This indicates that loss of PAX6 diverted only a subset of progenitors to an inhibitory
263 cell fate. We wondered whether PAX6 loss also affected the maturation trajectory of those
264 excitatory neurons that are still being generated. To address this, we furthered our analysis
265 into the excitatory neuronal clusters EN1 and EN2 (Fig 3). The majority of excitatory neurons
266 in *PAX6*$^{-/-}$ organoids fell into cluster EN1 which was also found in controls (Fig 3C), indicating

267 that these cells are transcriptionally similar to *PAX6*$^{+/+}$ cells. However, the number of EN2 cells
268 were substantially increased (~25 fold) in *PAX6*$^{-/-}$ organoids compared to controls (Fig 3C)
269 suggesting that PAX6 promotes a subset of neural progenitors to acquire EN2 cell fate. How
270 different are the cells in the EN2 cluster compared to EN1?
271
272 Highly expressed marker genes in EN2 cells include *NRXN1*, *CAMK4*, *DCC*, and *NDST3* which
273 are all involved in cellular signalling. Further, key marker genes for excitatory neurons such as
274 *NEUROD2* and *NEUROD6* (Bhaduri et al., 2020) are expressed at lower levels in EN2 cells than
275 in EN1 (Supplementary Table 1, Supplementary Data). However, EN2 cells do express
276 glutamate receptor genes including *GRID1*, *GRIK2* and *SHISA6* (Supplementary Table 1),
277 characteristic of excitatory glutamatergic neurons. DGE analysis between EN2 and EN1 cells
278 revealed higher levels of inhibitory marker genes including *DLX5* and *ASCL1*, and genes
279 involved in cellular signalling including *NRXN1*, *PXDC1*, *ADAM22* (and many more) in EN2 cells
280 (Fig 5A). Taken together, these findings indicate that a subset of excitatory neurons generated
281 in *PAX6*$^{-/-}$ organoids have an atypical transcriptome, expressing both excitatory and inhibitory
282 neuronal marker genes, perhaps as a consequence of dysregulated signalling and/or
283 dysregulated cellular response to signalling.
284
285 To determine whether PAX6 loss affects the lineage progression of excitatory neurons in
286 organoids, we assessed the maturation of the excitatory lineage in both *PAX6*$^{+/+}$ and *PAX6*$^{-/-}$
287 organoids using pseudotime. EN1 and EN2 were grouped together as excitatory neurons for
288 this analysis as there were insufficient EN2 cells in *PAX6*$^{+/+}$ organoids to allow a meaningful
289 comparison. We found that *PAX6*$^{+/+}$ organoids contained more mature cells of the excitatory
290 lineage than *PAX6*$^{-/-}$ organoids, as visualised by cell density along pseudotime (Fig 5B). Taken
291 together, these results indicate that in addition to diverting a subset of cortical progenitors
292 into an inhibitory lineage with an abnormal identity, loss of PAX6 results in a delay in the
293 maturation of excitatory neurons and enrichment of a particular subset of excitatory neurons,
294 EN2. This enrichment of EN2 however did not increase the proportion of total excitatory
295 neurons in *PAX6*$^{-/-}$ organoids.
296
297 ***Cell fate diversification in PAX6*$^{-/-}$ *cerebral organoids may be driven by a dysregulated***
298 ***response to intercellular signalling.***

299 To address the mechanism underlying these cell fate diversifications caused by loss of PAX6,
300 we identified genes which drive the diversification from excitatory to inhibitory cell fate in
301 *PAX6*$^{-/-}$ organoids. We used scFates to infer developmental trajectories of RGPs (Faure et al.,
302 2023) by computing pseudotime using RGP as a root node (Fig 6A-C). RGPs progressed
303 towards either an excitatory (Fig 6D) or an inhibitory neuronal fate (Fig 6F). To identify driver
304 genes in excitatory and inhibitory cell lineages, we performed DGE analysis along both
305 developmental trajectories. Driver genes display dynamic, highly variable expression changes
306 in the excitatory (Fig 6E) and inhibitory branches (Fig 6G). Plotting the expression of these
307 genes along pseudotime for each branch, we found that they can be grouped into two
308 categories: well-known marker genes for respective lineages and genes related to cellular
309 signalling. For example, we identified marker genes for excitatory fate such as *NEUROD6* and
310 *NEUROD2* (Fig 6E); and *DLX6-AS1*, *DLX5* and *ERBB4* for inhibitory fate (Fig 6G). Further, we
311 found genes related to cellular signalling including *PTPRZ1*, *DLGAP1*, *THSD7A*, *DAB1* in the
312 excitatory branch (Fig 6E); and *PDZRN3*, *SNTG1*, *NRXN3* in the inhibitory branch (Fig 6G). We
313 chose to focus further analysis on the *PTPRZ1* pathway as this emerged as the top candidate
314 driver gene in the excitatory trajectory (Fig 6E).
315
316 ***Decreased sensitivity to PTN-PTPRZ1 signalling in PAX6*$^{-/-}$ *cerebral organoids results in***
317 ***altered excitatory/inhibitory neuronal ratio.***
318 Protein tyrosine phosphatase receptor type Z1 (PTPRZ1) is a receptor for pleiotrophin (PTN)
319 (Meng et al., 2000; Wang, 2020). PTPRZ1 is highly expressed in cortical progenitors, especially
320 in oRGs, a progenitor cell type rarely found in mice but which is greatly expanded in primates
321 (Pollen et al., 2015). PTN signalling has been implicated in neuronal development (Garcia-
322 Gutierrez et al., 2014; Tang et al., 2019) and neurite outgrowth (Yanagisawa et al., 2010) but
323 it has not previously been studied in the context of cortical development. To investigate
324 whether the PTN-PTPRZ1 signalling pathway or the cellular response to PTN is dysregulated
325 in *PAX6*$^{-/-}$ organoids, we first examined expression of *PTN* and its receptor *PTPRZ1* (Fig 7A-F).
326 We saw no significant difference in *PTN* expression between *PAX6*$^{+/+}$ and *PAX6*$^{-/-}$ organoids (Fig
327 7A-C) but there was an overall decrease in *PTPRZ1* expression across all individual cell types
328 in *PAX6*$^{-/-}$ organoids compared to controls (Fig 7D-F). In addition to PTPRZ1, PTN has been
329 reported to interact with other cell surface receptors including ALK, SDC1, SDC2, SDC3, PTPRS,
330 PTPRB, PLXNB2, CDH10 and NCL (González-Castillo et al., 2015; Wang, 2020). To be

331 comprehensive, we also examined the mRNA expression of these receptors in our scRNAseq
332 dataset, which revealed no significant differences between *PAX6*$^{+/+}$ and *PAX6*$^{-/-}$ organoids
333 (Supplementary Fig 4).
334
335 We hypothesised that the lowered expression of *PTPRZ1* in *PAX6*$^{-/-}$ organoids could decrease
336 their sensitivity to PTN signalling, leading to the misspecification of RGPs from excitatory to
337 inhibitory fate. To test this possibility, we treated *PAX6*$^{+/+}$ and *PAX6*$^{-/-}$ organoids with PTN at an
338 earlier developmental age (organoid day 20) that precedes our observations described above.
339 After seven days, the ratio of inhibitory (DLX2+) to excitatory (TBR2+) cells was determined,
340 as a readout of PTN-PTPRZ1 signalling sensitivity (Fig 7K). Treating *PAX6*$^{+/+}$ organoids with 50
341 ng/ml PTN (Fig 7G-H) resulted in a statistically significant 2.75-fold decrease (6.27 to 2.28) in
342 the ratio of DLX2+/TBR2+ cells compared to vehicle treatment (Fig 7L). A surprising
343 observation that we noted was the similarity of the DLX2/TBR2 before PTN treatment
344 between D20 control and mutant organoids given that we described there were not many
345 DLX2+ cells in D60 control organoids resulting in a stark difference in DLX2/TBR2 ratio between
346 the control and *PAX6*$^{-/-}$ mutant D60 organoids (Fig 2-3). This difference likely reflects the
347 developmental trajectory of cerebral organoids: early-stage organoids (<2 months) contain
348 diverse cell types from multiple nervous system regions, including non-cortical cells, before
349 transitioning to exclusively cortical cell types by ~2 months/D60 (Uzquiano et al., 2022). This
350 possibly explains why DLX2+ cells were present at D20 but drastically reduced at D60 in
351 *PAX6*$^{+/+}$ control organoids resulting in a similar DLX2/TBR2 ratio between control and *PAX6*$^{-/-}$
352 mutant at D20 but not at D60.
353
354 Therefore, in the presence of PAX6, progenitor cells respond to the activation of the PTN-
355 PTPRZ1 pathway by committing to an excitatory rather than inhibitory fate. However, treating
356 *PAX6*$^{-/-}$ organoids with the same dose of PTN (Fig 7I-J) resulted in no change in the ratio of
357 DLX2+/TBR2+ cells (Fig 7L) most probably due to lowered expression of PTPRZ1 rendering the
358 cells less likely to respond to PTN. This indicates that dysregulated cellular response to PTN-
359 PTPRZ1 signalling due to the loss of PAX6 contributes to the misspecification of RGPs from
360 excitatory fate to inhibitory fate, thus altering the excitatory/inhibitory ratio.
361
362 ***Discussion***

363

364 Here, we have shown that PAX6 loss in human cerebral organoids leads to a subset of cortical
365 progenitors deviating from excitatory to inhibitory fate, resulting in an altered excitatory to
366 inhibitory neuronal ratio. The inhibitory cells generated from *PAX6*$^{-/-}$ physically segregate from
367 excitatory cells, forming separate territories. While excitatory neurons were still generated in
368 the absence of PAX6, their maturation appeared to be delayed and we found enrichment of
369 transcriptomically atypical excitatory cells that show upregulated expression of inhibitory
370 marker genes such as *ASCL1* and *DLX5* and genes important for cellular signalling such as
371 *NRXN1*, *PXDC1*, *ADAM22*. Finally, we present evidence of dysregulated cellular response to
372 the PTN-PTPRZ1 pathway in neural progenitors as a mechanism contributing to the altered
373 excitatory to inhibitory neuronal ratio in *PAX6*$^{-/-}$ organoids.

374

375 *PAX6 mediated regulation of excitatory/inhibitory neuronal fate across model systems*
376 Previously, we described Pax6's role in ensuring that mouse cortical progenitors progress
377 toward an excitatory neuronal fate by modulating the competence of the progenitors to
378 respond to the signalling molecules Sonic Hedgehog (Shh), which promotes the adoption of
379 inhibitory neuronal fate and Bone Morphogenetic Protein (BMP) which promotes excitatory
380 neuronal fate without any detectable changes in the expression of the ligand or receptors for
381 Shh or BMP. The result of this dysregulation in neural progenitors' competence to respond to
382 Shh and BMP was an increase of progenitors adopting inhibitory cell fate in the expense of
383 excitatory cell fate (Manuel et al., 2022).

384

385 Our present study using human organoids showed that the effect of PAX6 loss on the
386 excitatory/inhibitory neuronal ratio looks to be conserved across species. It also highlighted
387 some possible differences between the two model systems. We showed that dysregulated
388 neural progenitor response to the PTN-PTPRZ1 signalling pathway contributed to the altered
389 excitatory/inhibitory neuronal ratio in *PAX6*$^{-/-}$ organoids, most likely due to reduced
390 expression of the PTPRZ1 receptor. PTPRZ1 is normally highly expressed in human/primate
391 oRGs, a progenitor population that is not readily found in mice and PTN has been reported to
392 act as a trophic factor responsible for maintaining the oRG stem cell niche (Pollen et al., 2015).
393 While we did not annotate oRGs separately from RGPs in our scRNAseq dataset, there are
394 oRGs present in both *PAX6*$^{+/+}$ and *PAX6*$^{-/-}$ organoids as shown by the expression of the oRG

395 markers *HOPX*, *PTPRZ1*, *FAM107A* (Pollen et al., 2015) (Supplementary Fig 5B). The data we
396 obtained suggests that PTN-PTPRZ1 signalling could be a possible human-specific mechanism
397 of action underlying the altered excitatory/inhibitory ratio in *PAX6*$^{-/-}$ organoids as *Ptprz1* was
398 not found to be differentially expressed between wildtype and Pax6 cortex-specific knockout
399 mice (Manuel et al., 2022).
400
401 *PTN-PTPRZ1 role in cell fate commitment*
402 The neurotrophic factor PTN is highly expressed in neural stem cells in the adult hippocampus
403 and facilitates the maturation of newborn neurons (Tang et al., 2019). Part of its role in
404 maturation includes the stimulation of neurite outgrowth (Yanagisawa et al., 2010) however,
405 it has not previously been implicated in cell fate specification - specifically neurons of
406 excitatory or inhibitory fate as shown in this study. Cell cycle length can contribute to changes
407 in cell fate, for example in the process of Yamanaka reprogramming in which somatic cells
408 undergo an ultrafast cell cycle of about 8 hours/cycle (Chen et al., 2015). Therefore, PTN-
409 PTPRZ1 signalling could affect neural cell fate specification by influencing the rate of
410 proliferation or cell cycle time. PTN's actions on proliferation and cell cycle are context
411 dependent. PTN signalling is needed for cell cycle progression in glioblastoma cells as it can
412 stimulate glioblastoma stem cells during tumour growth (Chang et al., 2006; Shi et al., 2017),
413 promote proliferation of neural stem and progenitor cells in the hippocampus (Li et al., 2023).
414 In other cell types such as bovine chondrocytes, PTN inhibits proliferation (Tapp et al., 1999).
415 Further experimentation will be required to fully describe the molecular pathway by which
416 PTN-PTPRZ1 signalling influences cortical excitatory/inhibitory neural fate specification. It is
417 possible that changes in other signalling pathways contribute to the altered
418 excitatory/inhibitory neuronal ratio in *PAX6*$^{-/-}$ organoids as cell fate commitment is a complex
419 process and likely involves many other factors and cofactors. PTN-PTPRZ1 signalling is almost
420 certainly only one piece of a complex puzzle. Other signalling-related genes that were
421 differentially expressed in *PAX6*$^{-/-}$ cells differentiating along the inhibitory pathway included
422 *PDZRN3*, *SNTG1* and *NRXN3* (Supplementary Fig 5A) though experimental validation of these
423 findings is beyond the scope of this study.
424
425 *Atypical inhibitory and excitatory cells generated in PAX6*$^{-/-}$ *organoids*

426 We described inhibitory cells and a subset of excitatory cells, EN2, generated in *PAX6*$^{-/-}$
427 organoids showing atypical transcriptomic profile. Some gene expression differences between
428 cells in organoids and cells in embryos are to be expected, given likely differences between
429 the *in vitro* culture environment and fetal environment *in vivo*. However, given the
430 dysregulation in *PAX6*$^{-/-}$ cells' cellular response to PTN-PTPRZ1 signalling resulting in altered
431 excitatory/inhibitory ratio of neurons, we consider that it is more likely that PAX6 loss resulted
432 in the generation of neurons that express inhibitory identity genes in the case of inhibitory
433 neurons and excitatory identity genes for the subset of excitatory neurons in the EN2 cluster
434 but are abnormal in their ability to interact with intra and intercellular signalling pathways due
435 to differences their molecular features compared to *in vivo* inhibitory or excitatory neurons
436 respectively.
437
438 In the case of the inhibitory neurons, previous reports suggested that *Pax6* deletion in mice
439 resulted in the generation of immature olfactory bulb INs that are marked by the expression
440 of the genes *Sp8, Scgn, Calb2* and *Tshz1* (Guo et al., 2019; Kroll and O'Leary, 2005). However,
441 our previous study on *Pax6* deletion in mouse cortical progenitors produce inhibitory neurons
442 that showed a different response to *Gsx2* loss to normal dLGE cells, cells that would mature
443 into olfactory bulb INs indicating that the inhibitory neurons in *Pax6*$^{-/-}$ mice are abnormal.
444 Results from the current study supports the latter suggestion as while PAX6 deletion in
445 organoids generated INs, they showed an atypical transcriptomic profile. We further assessed
446 for olfactory bulb IN identity cells (cells that co-express *SP8* and *SCGN*; *SP8*, *CALB2* and *TSHZ1*)
447 in our scRNAseq dataset but we did not find many, if any, cells at all (Supplementary Fig 5D-
448 E). Further, the extreme segregation from other cell types in the organoid also supports the
449 idea that these inhibitory cells are abnormal with an aberrant transcriptomic profile as normal
450 inhibitory neurons integrate into the developing cerebral cortex *in vivo* and in
451 organoid/assembloid models (Osaki et al., 2024; Sharf et al., 2022; Wang et al., 2025b).
452

453 **Figure legends**

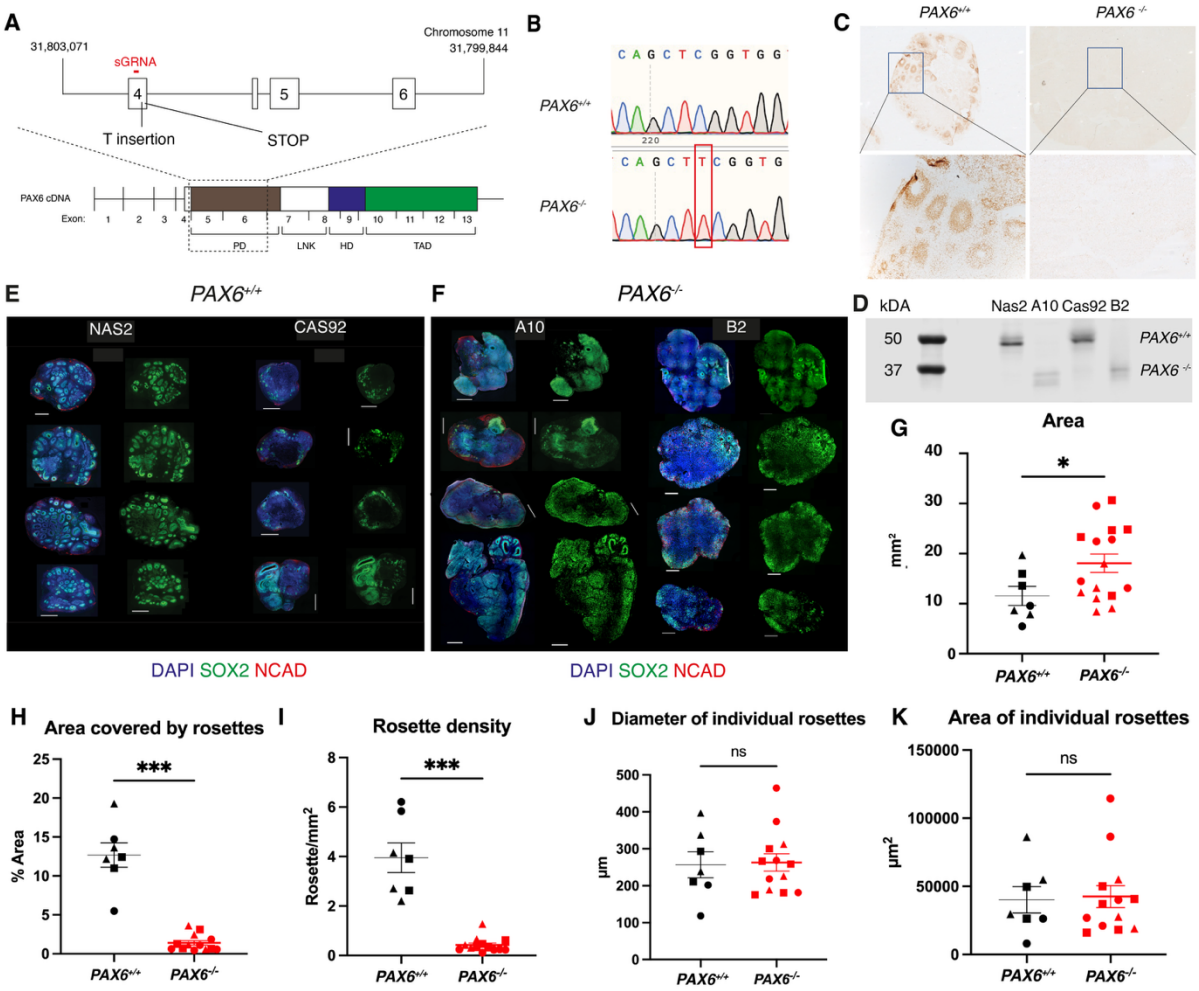

454

455 **Fig 1** (A) Diagram showing part of the human *PAX6* locus indicating the location and nature of
456 the mutation introduced to the *PAX6*$^{-/-}$ iPSC lines. Homozygous insertion of a single T residue
457 in exon 4 caused a frameshift mutation leading to a premature stop codon within exon 4.
458 Exons 1-3 are non-coding. PD – paired domain; LNK – linker; HD – homeodomain; TAD –
459 transactivation domain. (B) Sanger sequencing of *PAX6*$^{-/-}$ iPSC genomic DNA showing the T
460 insertion mutation. (C) PAX6 PD immunostaining of day 60 control and *PAX6*$^{-/-}$ organoids,
461 confirming PAX6 PD domain absence in mutants. (D) Western blot showing PAX6 protein
462 expression in *PAX6*$^{-/-}$ iPSCs, A10 and B2 and control lines Nas2 and Cas92. (E,F) SOX2 and N-
463 CAD Immunostaining of representative sections of individual day 60 control and *PAX6*$^{-/-}$
464 organoids from separate differentiation batches (4). Scale bar = 1 mm. DAPI in blue, SOX2 in
465 green, NCAD in red (G) Quantification of cross-sectional area of day 60 control and *PAX6*$^{-/-}$
466 organoids, p = 0.025 (H–K) Quantification of organoid size and rosette characteristics. (H) Area
467 covered by rosettes between genotypes is significantly different with p = 0.0003. (I) Rosette

density between genotypes was also significantly different with $p = 0.001$. (J – K) Neither the diameter or area of individual rosettes was significantly different between genotypes ($p = 0.88$ and $p = 0.85$ respectively). Each symbol represents an individual organoid while triangles, dots and square symbols indicate separate organoid batches. $N \geq 7$ organoid batches. Each data point shown here consists of an average of 3 organoids per batch. * denotes significant difference of $p < 0.05$.

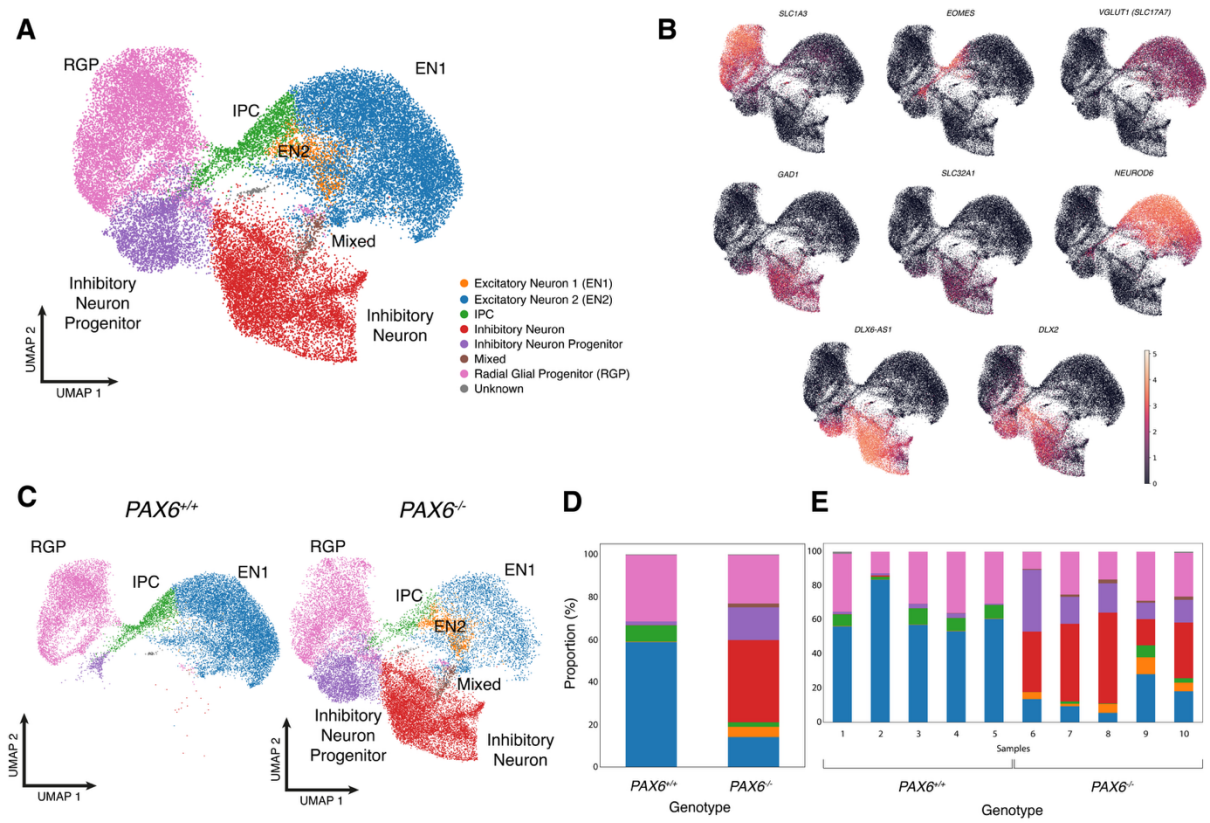

Fig 2 (A) UMAP plot showing combined scRNAseq data from day 60 *PAX6*$^{-/-}$ and control organoids. RGP – Radial glia progenitor; IPC – Intermediate progenitor cells; EN1 – excitatory neuron 1, EN2 – excitatory neuron 2. (B) UMAPs showing selected marker gene expression in specific cell types in day 60 organoids. (C) Separate UMAP plots of scRNAseq data from control (left) and *PAX6*$^{-/-}$ (right) organoids. (D-E) Comparison of cell type composition between control and *PAX6*$^{-/-}$ day 60 organoids showing all cell types coloured as in previous panels (A). (D) Comparison of cell types between *PAX6*$^{+/+}$ and *PAX6*$^{-/-}$ (E) shows cell compositions of individual samples

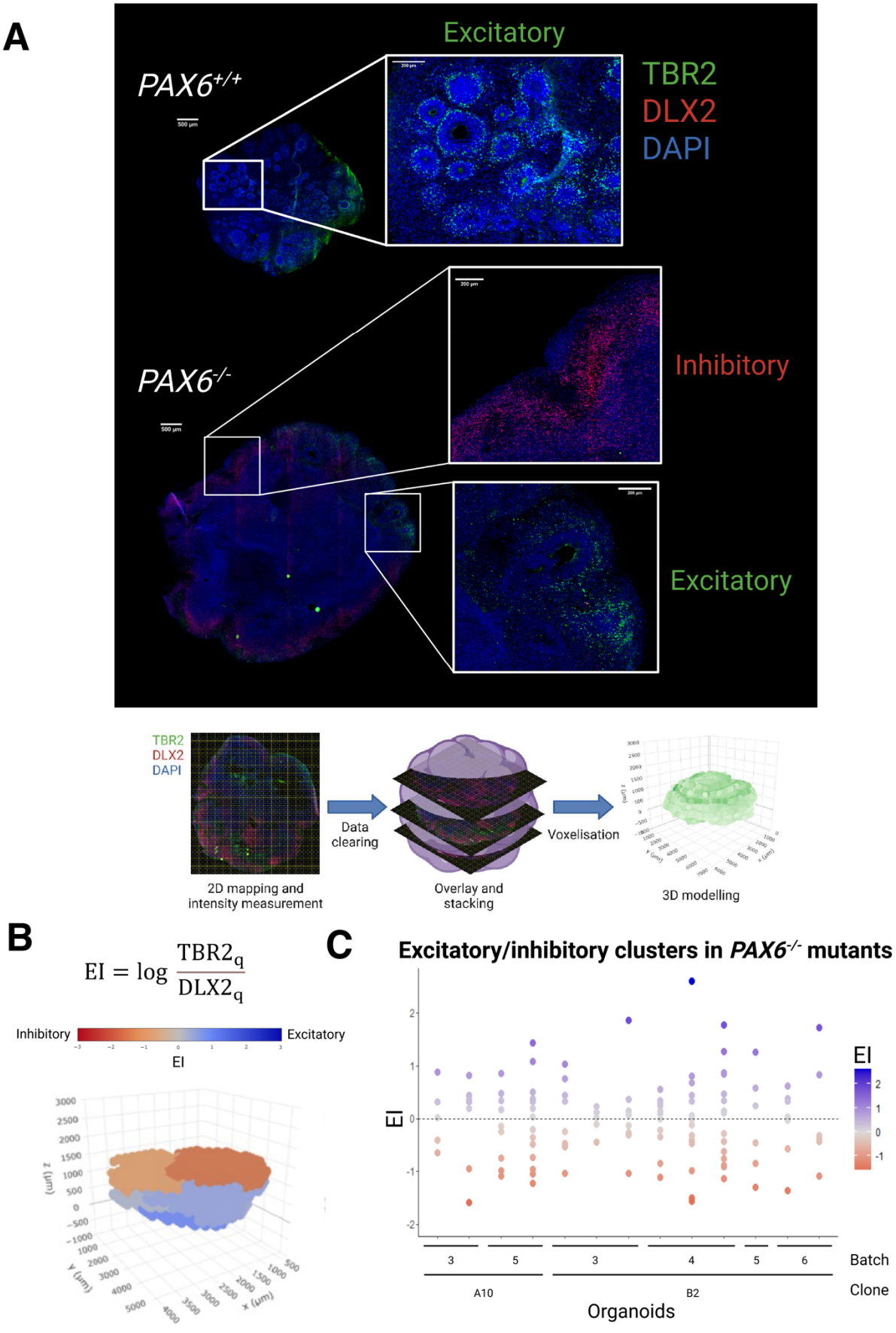
A
Excitatory
PAX6+/+
TBR2
DLX2
DAPI
PAX6-/-
Inhibitory
Excitatory
TBR2
DLX2
DAPI
Data clearing
Voxelisation
2D mapping and intensity measurement
Overlay and stacking
3D modelling
B
EI = log TBR2q / DLX2q
Inhibitory
Excitatory
EI
C
Excitatory/inhibitory clusters in PAX6-/- mutants
EI
Batch
Clone
A10
B2
Organoids

485

Fig 3 (A) Schema outlining method for production and quantitation of 3D models of organoids. Sections were immunostained for TBR2 and DLX2 and processed as shown. (B) Equation by which excitatory/inhibitory identities were conferred upon specific territories in organoids and (C) graph summarising the segregation of these territories in individual organoids.

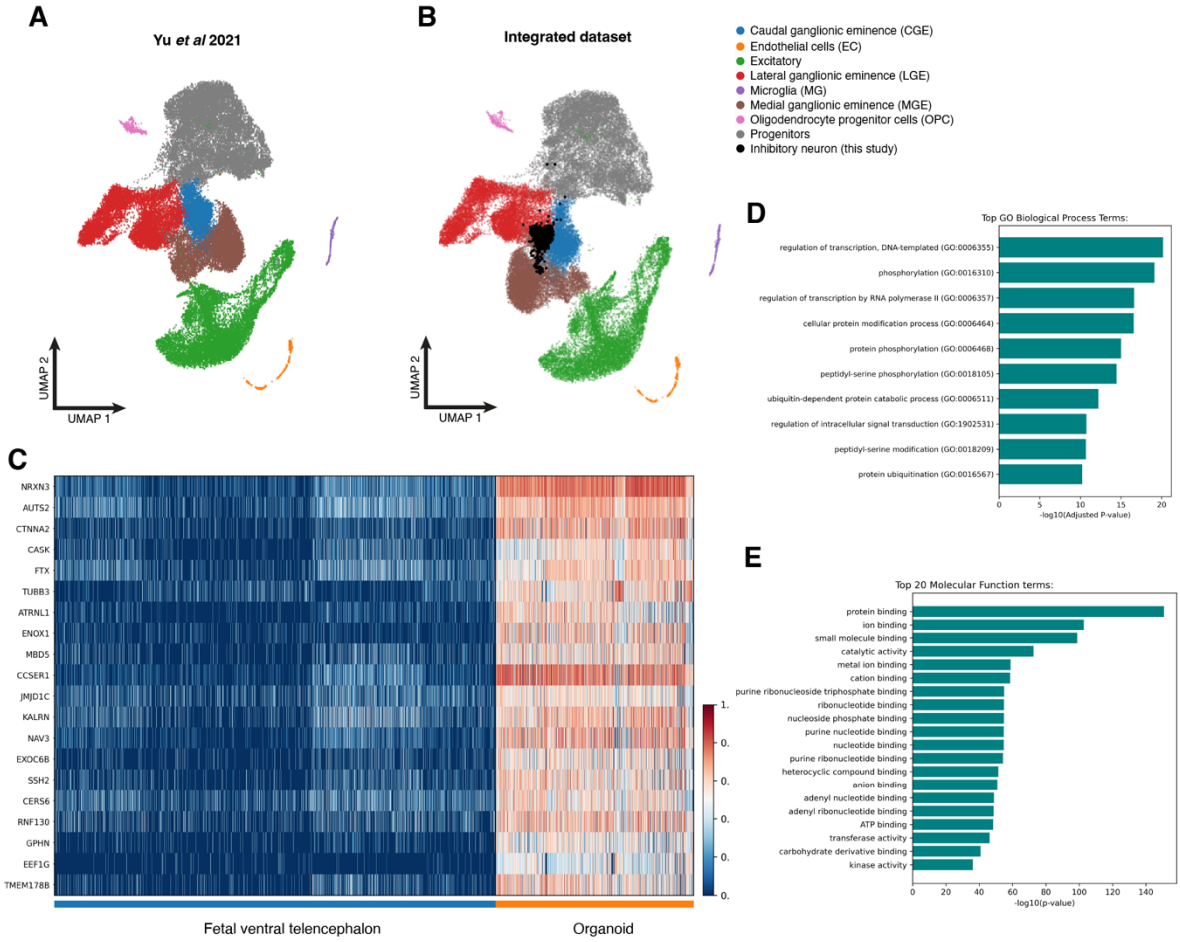

Fig 4 (A) scRNAseq dataset of fetal ganglionic eminences from (Yu et al., 2021). (B) Integrated dataset of inhibitory neurons (black) found in this study with the dataset from (A) showing that inhibitory neurons found in *PAX6*$^{-/-}$ organoids do not cluster to a specific inhibitory subtype found in *in vivo* fetal ganglionic eminences but a mixture of subtypes. (C) Heatmap showing top 20 DEGs between the inhibitory neurons from *PAX6*$^{-/-}$ organoid and fetal ventral telencephalon. (D) Top 10 biological process GO terms from the list of DEGs between *PAX6*$^{-/-}$ organoid and fetal inhibitory neurons. (E) Top 20 molecular function GO terms from the list of DEGs between *PAX6*$^{-/-}$ organoid and fetal inhibitory neurons.

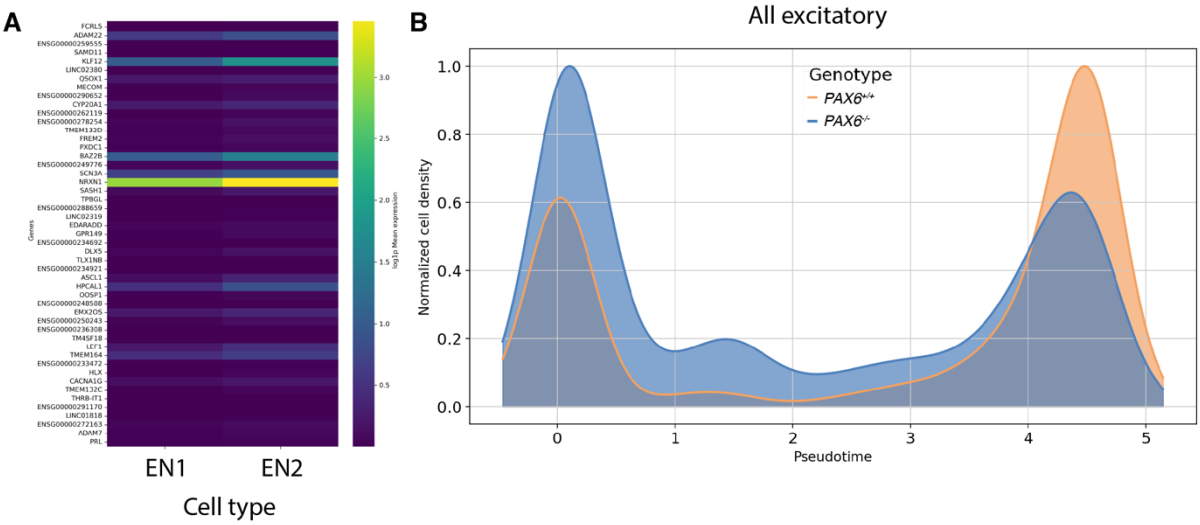

Fig 5 (A) Differential gene expression between EN1 and EN2 excitatory neuron clusters showing higher expression of inhibitory marker genes and genes involved in cellular signalling in EN2. (B) Pseudotime plot of excitatory lineage cells showing the developmental progression from progenitor to excitatory neurons. *PAX6*$^{+/+}$ is shown in orange and *PAX6*$^{-/-}$ is shown in blue, showing that *PAX6*$^{-/-}$ organoids have more immature cells along the excitatory lineage than do *PAX6*$^{+/+}$organoids.

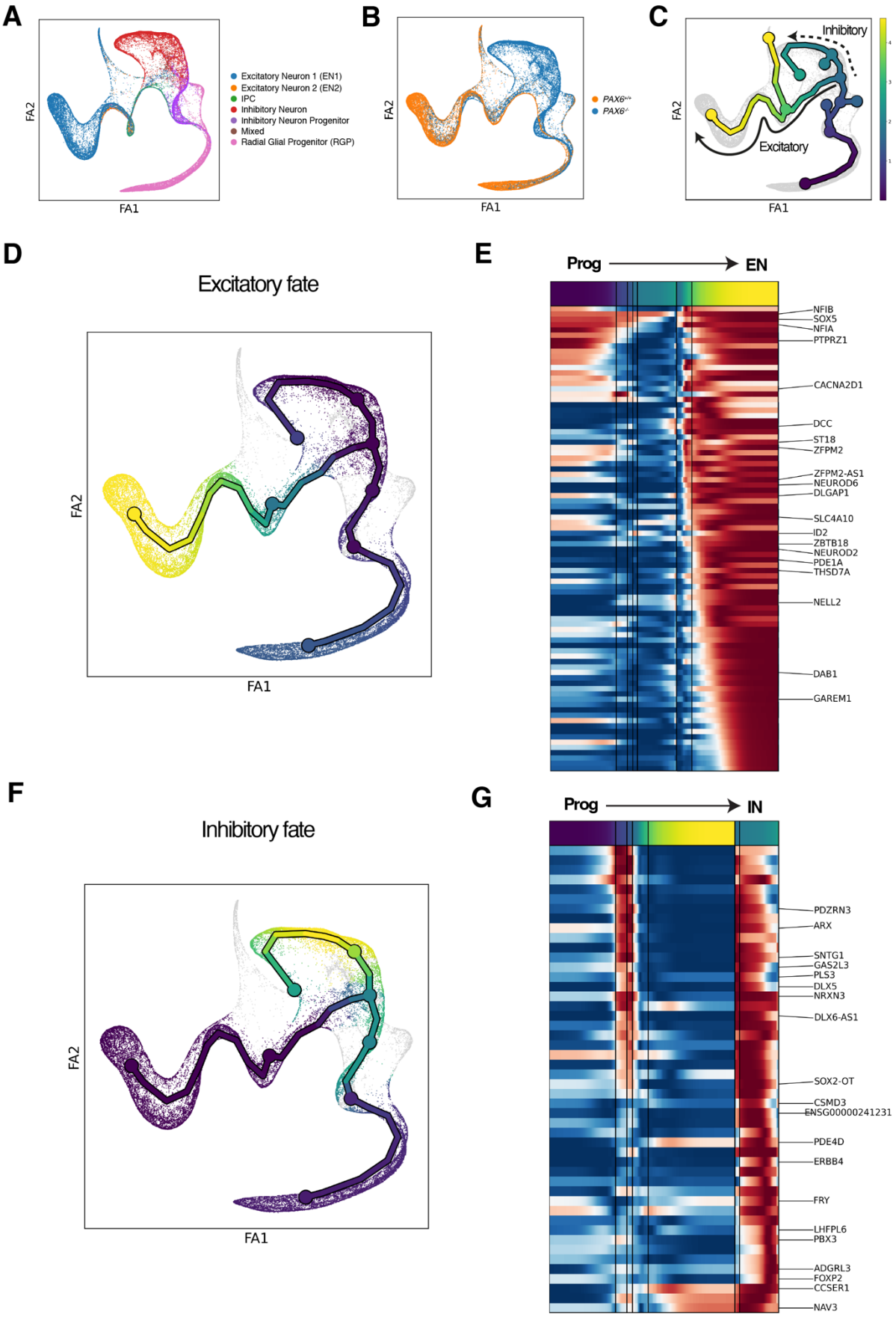
A
FA2
FA1
Excitatory Neuron 1 (EN1)
Excitatory Neuron 2 (EN2)
IPC
Inhibitory Neuron
Inhibitory Neuron Progenitor
Mixed
Radial Glial Progenitor (RGP)
B
FA2
FA1
PAX6+/+
PAX6-/-
C
Inhibitory
Excitatory
FA2
FA1
D
Excitatory fate
FA2
FA1
E
Prog
EN
NFIB
SOX5
NFIA
PTPRZ1
CACNA2D1
DCC
ST18
ZFPM2
ZFPM2-AS1
NEUROD6
DLGAP1
SLC4A10
ID2
ZBTB18
NEUROD2
PDE1A
THSD7A
NELL2
DAB1
GAREM1
F
Inhibitory fate
FA2
FA1
G
Prog
IN
PDZRN3
ARX
SNTG1
GAS2L3
PLS3
DLX5
NRXN3
DLX6-AS1
SOX2-OT
CSMD3
ENSG00000241231
PDE4D
ERBB4
FRY
LHFPL6
PBX3
ADGRL3
FOXP2
CCSER1
NAV3

510

511 **Fig 6** (A) Force-directed graph of scRNAseq data with cells arranged in pseudotime and
512 coloured according to their cell type. (B) Same graph as in (A) coloured according to genotype,
513 *PAX6*$^{+/+}$ in orange and *PAX6*$^{-/-}$ in blue. (C) Force-directed graph coloured in pseudotime with
514 early pseudotime in dark blue and later pseudotime in yellow. (D) Force-directed graph
515 showing excitatory differentiation trajectory and (F) inhibitory trajectory in pseudotime. (E)
516 Expression pattern of genes from progenitor to excitatory neurons that were differentially
517 expressed in the excitatory trajectory. (G) Expression pattern of genes from progenitor to
518 inhibitory neurons that were differentially expressed in the inhibitory trajectory. Prog –
519 progenitor; EN – excitatory neuron; IN – inhibitory neuron.
520

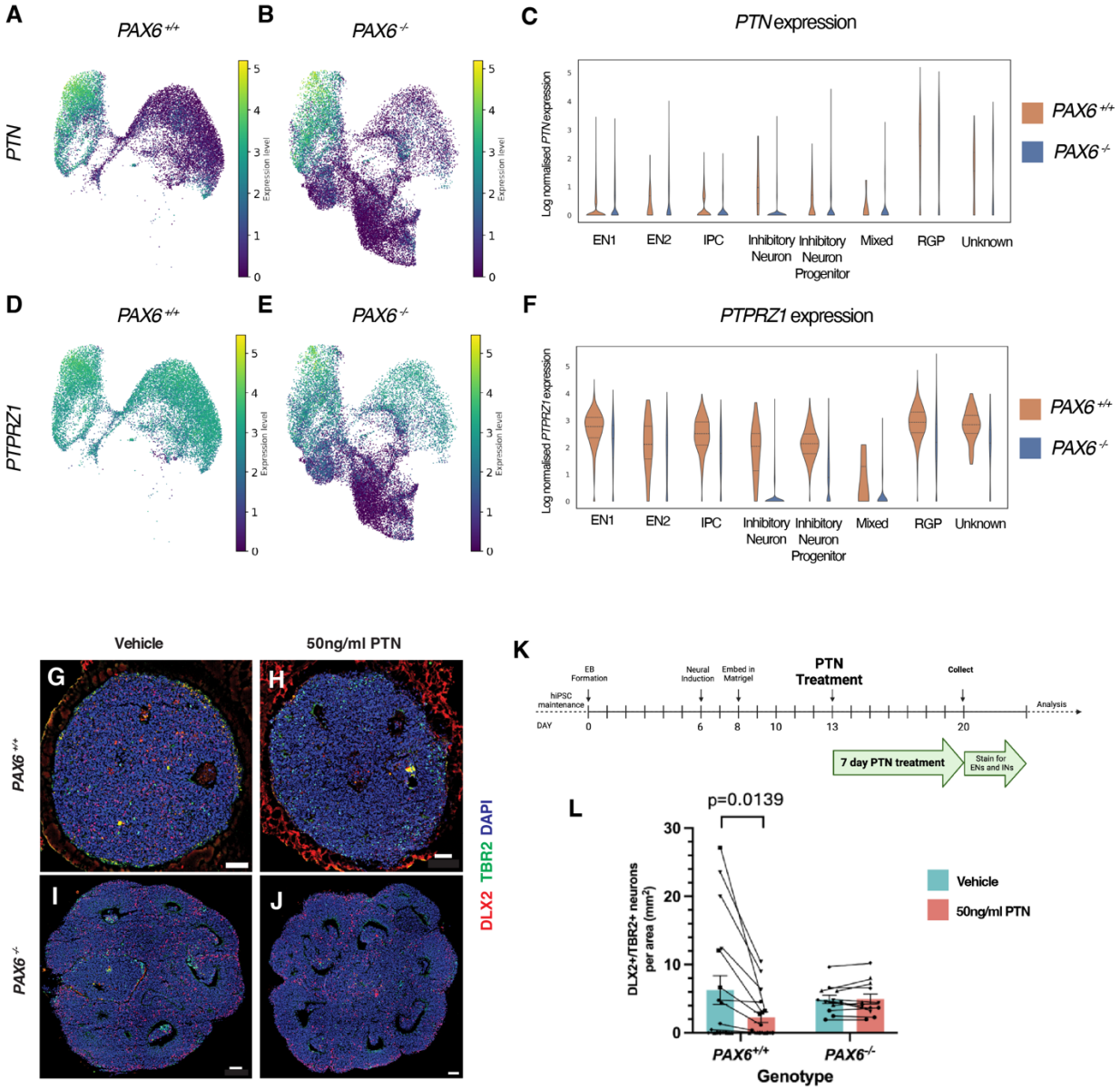

Fig 7 (A) UMAP plot of *PTN* expression in *PAX6*$^{+/+}$ and (B) in *PAX6*$^{-/-}$. (C) Violin plots of *PTN* expression across different cell types found in each genotype, *PAX6*$^{+/+}$ in brown and *PAX6*$^{-/-}$ in blue. (D) UMAP plot of *PTPRZ1* expression in *PAX6*$^{+/+}$ and (B) in *PAX6*$^{-/-}$. (C) Violin plots of *PTPRZ1* expression across different cell types found in each genotype, *PAX6*$^{+/+}$ in brown and *PAX6*$^{-/-}$ in blue. (G) Representative image of *PAX6*$^{+/+}$ organoid treated with vehicle and (H) treated with 50ng/ml PTN showing a decrease in DLX2+ cells (red). (I) Representative image of *PAX6*$^{-/-}$ organoid treated with vehicle and (J) treated with 50ng/ml PTN. (K) Schema showing PTN treatment timeline. (L) Quantification of DLX2+/TBR2+ cells per area after vehicle or PTN treatment.

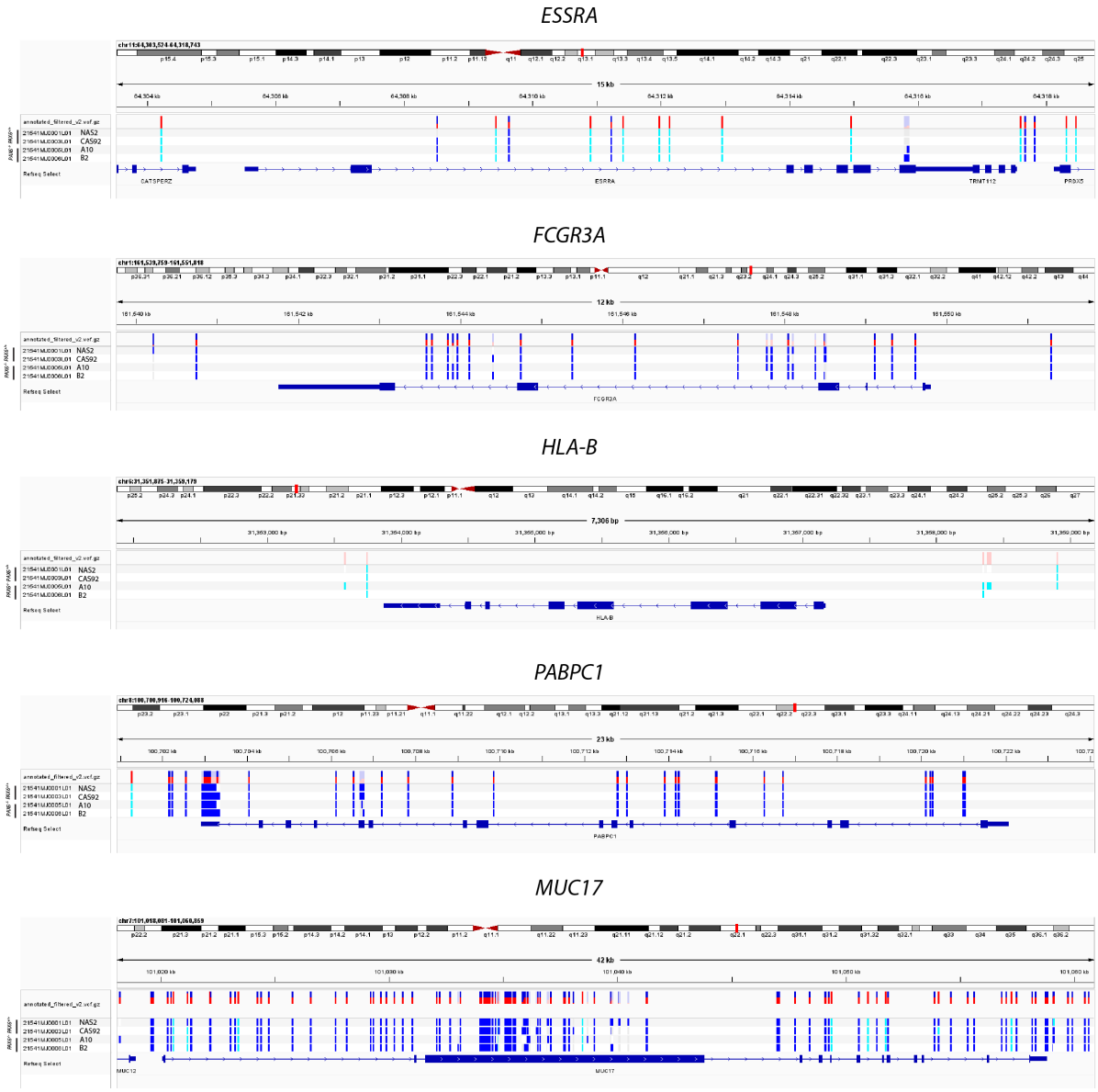

532

533

534 **Supplementary Fig 1.** Integrated Genomics Viewer (IGV) plots of genes with the highest
535 difference in mutation counts (SNV, indels, and point mutations) between *PAX6*$^{+/+}$ and *PAX6*$^{-/-}$
536 groups. Mutation variants for each individual samples are denoted as: homozygous variant –
537 cyan; heterozygous variant – blue while allele frequencies are denoted as: high allele
538 frequency of the variant – red; high allele frequency of reference sequence – blue. We
539 examined five genes that showed the highest difference in mutation counts between *PAX6*$^{+/+}$
540 and *PAX6*$^{-/-}$ which were *MUC17, PABPC1, ESSRA*, *FCGR3A* and *HLA-B*. *MUC17* mutations are
541 commonly found in iPSCs and have no reported effects on pluripotency or genomic integrity
542 (D'Antonio et al., 2018). Other than *MUC17*, no mutations were found in coding regions of
543 any of the other genes. Moreover, the variants reported by WGS were found in all four cell

544 lines (Supplementary Fig 1) signifying that they are background mutations (Young et al., 2012)
545 present in the parental line NAS2.
546

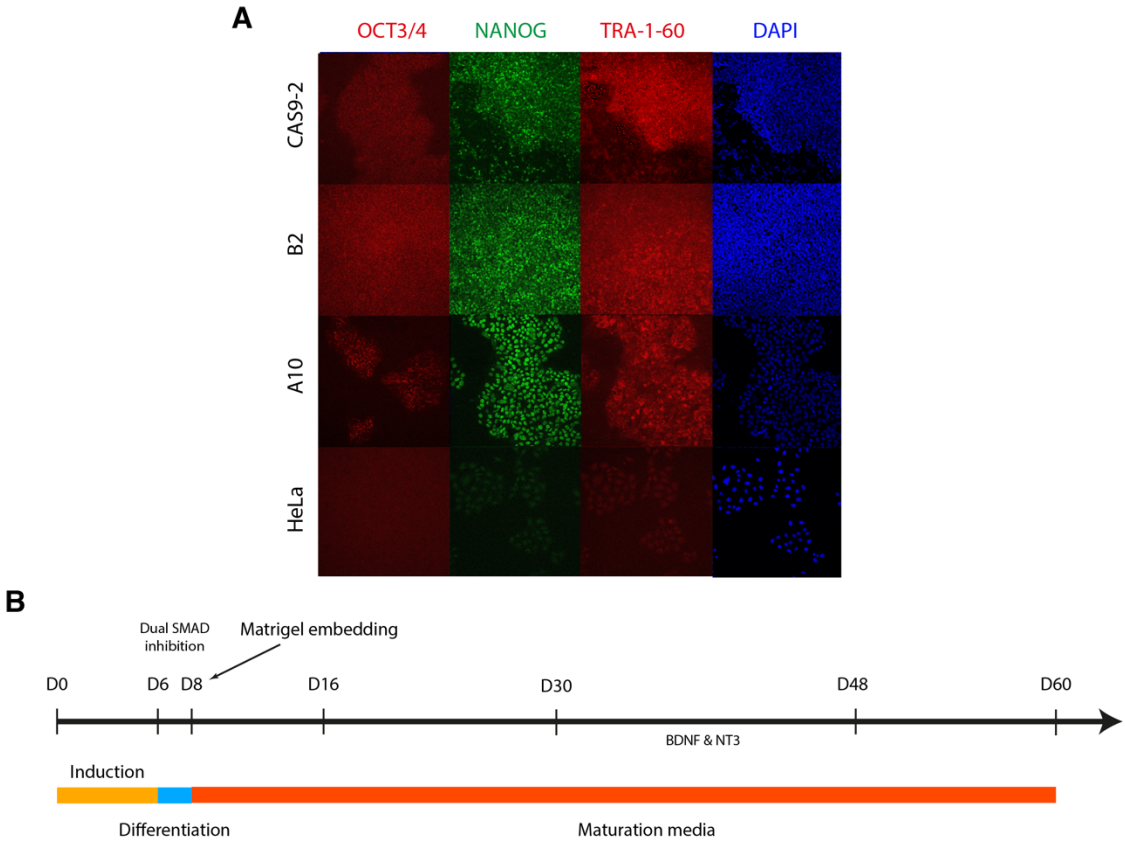

Supplementary Fig 2. (A) Immunostaining of CRISPR edited iPSC cell lines used in this study showing expression of pluripotency markers NANOG, OCT3/4 and TRA-1-60. HeLa cells were used as a negative control. (B) Timeline illustrating organoid differentiation protocol.

PAX6$^{-/-}$

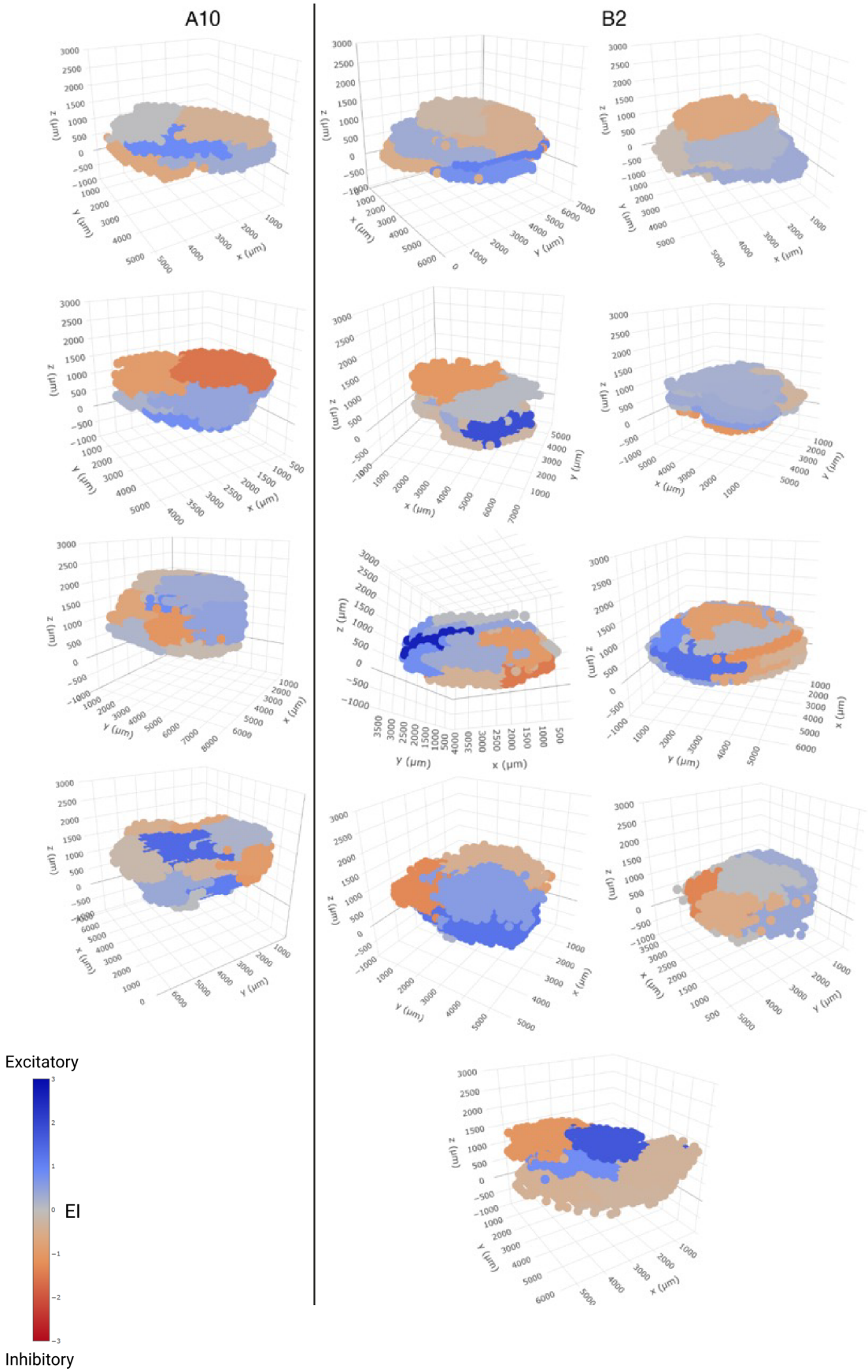

551

552 **Supplementary Fig 3.** 3D models of all individual organoids of both *PAX6*$^{-/-}$ clones (A10 and

553 B2) that were quantified.

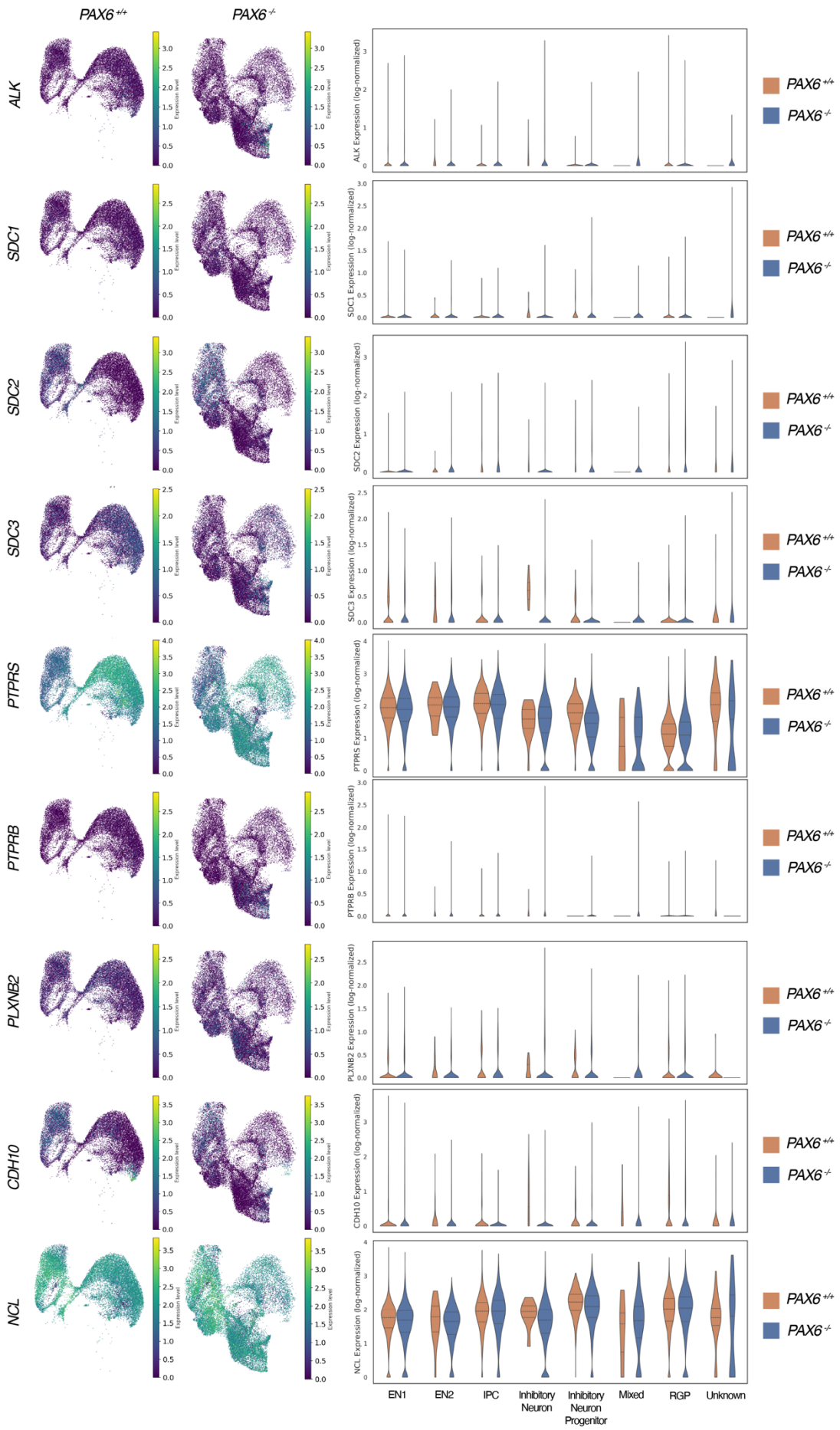
PAX6 +/+
PAX6 -/-
ALK
SDC1
SDC2
SDC3
PTPRS
PTPRB
PLXNB2
CDH10
NCL
Expression level
ALK Expression (log-normalized)
SDC1 Expression (log-normalized)
SDC2 Expression (log-normalized)
SDC3 Expression (log-normalized)
PTPRS Expression (log-normalized)
PTPRB Expression (log-normalized)
PLXNB2 Expression (log-normalized)
CDH10 Expression (log-normalized)
NCL Expression (log-normalized)
EN1
EN2
IPC
Inhibitory Neuron
Inhibitory Neuron Progenitor
Mixed
RGP
Unknown

554

555 **Supplementary Fig 4.** UMAP and violin plots showing expression of genes involved in the PTN
556 signalling pathway showing no differences between *PAX6*$^{+/+}$ and *PAX6*$^{-/-}$.
557

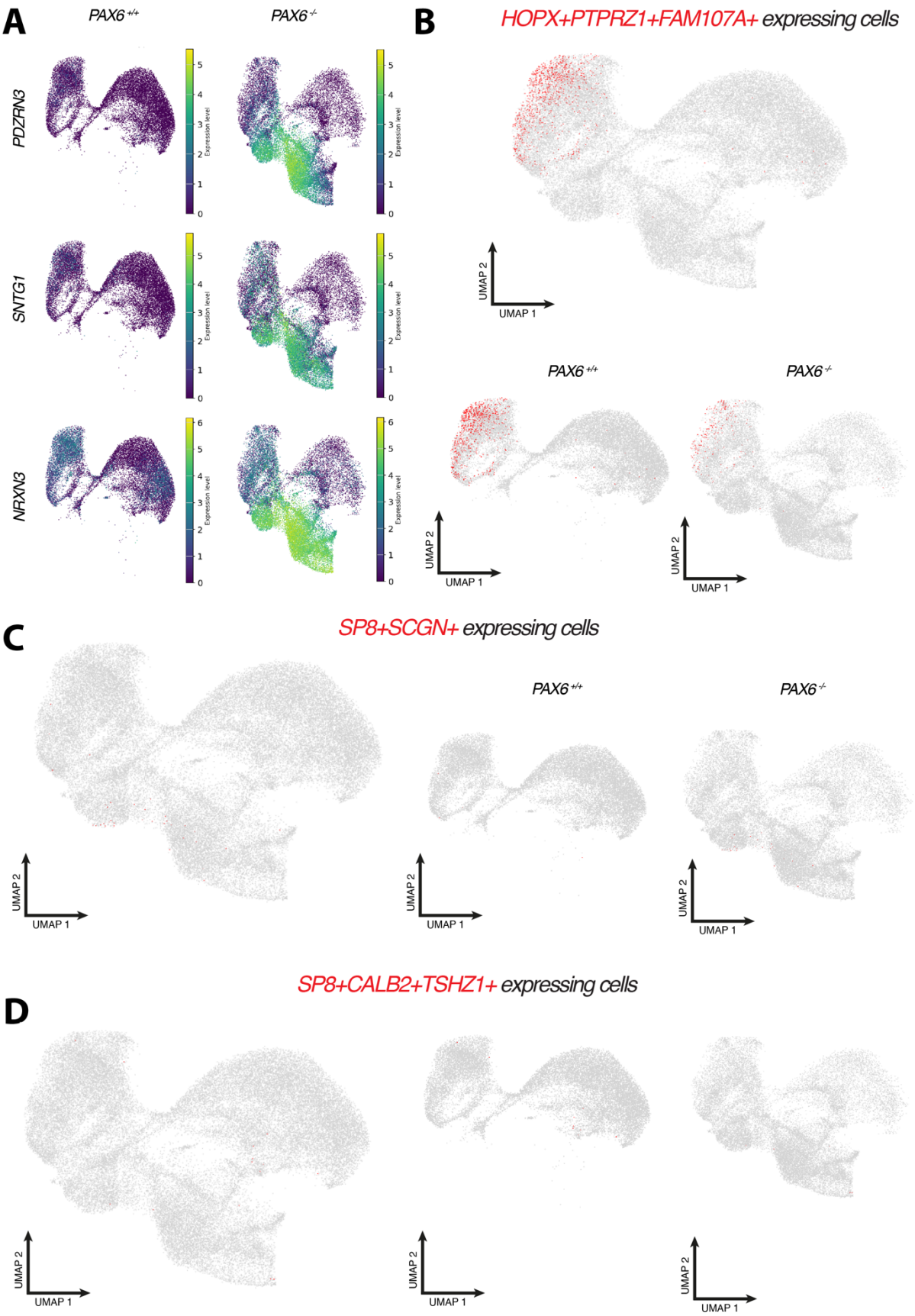

Supplementary Fig 5. (A) UMAP plots of cells expressing *PDZRN3*, *SNTG1* and *NRXN3* with higher expression in yellow and low expression in dark blue. (B) UMAP plots showing cells that

561 express oRG markers *HOPX*, *PTPRZ1*, and *FAM107A* (C) UMAP plots showing cells that co-
562 express *PAX6* and *MEIS2* (D) UMAP plots showing cells that co-express *SP8* and *SCGN* (E)
563 UMAP plots showing cells that co-express *SP8*, *CALB2* and *TSHZ1*.
564

Supplementary Table 1

Excitatory Neuron1	Excitatory Neuron2	IPC	Inhibitory Neuron	Inhibitory Neuron Progenitor	Mixed	RGP	Unknown
GRIA2	ZFPM2	CACNA2D1	NRXN3	HMGN2	H3-3B	GLI3	TALAM1
NEUROD2	NRXN1	PRDX1	DLX6-AS1	ATAD2	MALAT1	CREB5	CENPF
LRRC7	ZFPM2-AS1	NHLH1	SOX2-OT	SMC4	TALAM1	VIM	NFIA
PDE1A	ENSG00000285755	TENM4	DCX	HMGB2	EIF1	SHROOM3	PTPRD
NELL2	CBLB	HES6	DCLK2	TUBA1B	BNIP3L	MIR99AHG	ZFPM2
SLA	LINGO2	TMSB4X	PDZRN3	CENPU	ZFAS1	SFRP1	ENSG00000271860
NEUROD6	NYAP2	ELAVL4	SLAIN1	DLEU2	VEGFA	DACH1	H1-3
CACNA1E	CACNA2D1	SLCO5A1	CCSER1	TMPO	DDIT4	COL4A5	HDAC9
ZBTB18	CAMK4	NFIA	GAD2	HMGB1	RLF	SLC1A3	CTNND2
SLC24A2	SRRM4	IGFBPL1	ENSG00000239381	CENPF	YTHDC1	ENSG00000271860	THSD7A
THSD7A	DCC	EZR	DLX5	SMC2	KMT2E	TTYH1	OPCML
DAB1	SORBS2	ENSG00000231252	SOX4	RRM2	HSP90AB1	KIAA1217	H1-5
NFIB	GRID1	FYN	ENSG00000241231	KNL1	MATR3	NPAS3	KAZN
AFF3	BICD1	MARCKS	ENOX1	DIAPH3	ARID4B	IQGAP2	FOXG1
PPP2R2B	GRIK2	ELAVL2	CCDC88A	NUSAP1	CCNL1	PARD3B	CNTNAP2
LINC01122	RBFOX3	FOXN2	SNTG1	DEK	RSRC2	ID4	LINGO2
SH3GL2	SHISA6	PGAP1	ERBB4	LMNB1	RBM39	GULP1	DACH1
CNTNAP2	NDST3	CECR2	ATRNL1	EZH2	USPL1	DOK5	SOX5
RBFOX1	NFASC	EOMES	GAD1	TOP2A	OGA	COL4A6	DPP10
SLC4A10	PDE1A	CORO1C	ZNF704	H2AZ1	MORF4L2	ZFP36L1	LRRTM4

Supplementary Table 1. Marker genes of each cell type.

567 **Material & Methods**

568

569 *Cell culture and organoid generation*

570 iPSCs were maintained at 37°C with 5% CO_2 in StemMACS iPS-Brew XF (Miltenyi) on Laminin
571 521 (Biolamina) coated plates and passaged with 0.5 mM EDTA (Life Technologies). Organoids
572 were differentiated using a modified Lancaster protocol (Lancaster et al., 2013) which included
573 addition of 10 µM SB431542 (Tocris) and 100 nM LDN-193189 (APExBIO) for neural induction
574 and addition of 20 ng/ml BDNF and NT3 (Peprotech) to the medium at D30 for two weeks to
575 aid neuronal maturation (Supplementary Fig 2B). Briefly, 9000 cells were aggregated using
576 ultra-low attachment 96-well plates into embryoid bodies. These embryoid bodies were then
577 incubated in neural induction media containing dual SMAD inhibition as detailed above at day
578 six. Neural induction media was refreshed for day seven and organoids were embedded in
579 Matrigel on day eight. Organoids were transferred to an orbital shaker and maintained in 37°C
580 with 5% CO_2 incubators for 60 days. All media change were done every other day.

581

582 *CRISPR/Cas9 mutagenesis*

583 iPSCs were transfected with sgRNA 3' UCCCUUUCCUCAGGUCACAG 5' (Synthego) via
584 nucleofection using program CA137 on a 4D Nucleofactor X (Lonza) as per manufacturer's
585 instructions. Clones were obtained by single cell dissociation of the transfected pool followed
586 by screening for PAX6 mutation by Sanger sequencing of the *PAX6* locus. Successfully edited
587 clones were re-sequenced and pluripotency test were performed using STEMlight
588 Pluripotency kit (Invitrogen) (Supplementary Fig 1). Likely sites for off-target effects were
589 identified using Cas-OFFinder (http://www.rgenome.net/cas-offinder/) and annotated in
590 whole genome sequencing (WGS) data of all the iPSC lines. WGS data of all cell lines are
591 deposited in ENA (accession: PRJEB63603).

592

593 *Immunohistochemistry*

594 12µm thick cryosections of organoids were permeabilized in 0.1% Triton/PBS before
595 incubation with primary antibodies at 1/200 dilution using appropriate serum as blocking
596 buffer without antigen retrieval step: SOX2 (rabbit, ab92494 Abcam), TBR2 (sheep, AF6166
597 Bio-Techne), DLX2 (mouse, sc-393879 Santa Cruz); with antigen retrieval step: PAX6 (mouse,
598 AD2.38, described in Engelkamp et al., (1999)), NCAD (mouse, 610920 BD Biosciences). All

599 primary antibodies (except PAX6) were detected using AlexaFluor secondary antibodies
600 (Invitrogen) at 1/200 dilution. PAX6 was detected using Vectastain ABC kit (Vector Labs).
601 StemLight Pluripotency Antibody Kit (Stem Cell Technologies) was used for pluripotency
602 testing. All immunohistochemistry was performed on ≥ 3 sections of individual control and
603 *PAX6*$^{-/-}$ organoids. Number of organoids of each genotype ≥ 3 were used from ≥ 3
604 differentiation batches.
605
606 *Western blot*
607 Snap-frozen cells were homogenized in RIPA buffer [10 mM Tris-HCl, 140 mM NaCl, 1 mM
608 EDTA, 1% Triton X-100, 0.1% sodium DOC, 0.1% SDS, and Pierce protease inhibitor tablet,
609 EDTA-free (A32965, Thermo Fisher Scientific)] in a bead mill 24 homogenizer (Fisher Scientific).
610 Genomic DNA was removed with a Benzonase digest (E1014, Merck) for 15 min at room
611 temperature. Protein concentration was quantified using DC Bio-Rad II (5000112, Bio-Rad) in
612 a microtiter plate using a FLUOstar Omega plate reader (BMG Labtech). Samples were diluted
613 in one-third volume of 4× Laemmli buffer (0.5 M tris-HCl, 8% SDS, 0.01% bromophenol blue,
614 40% glycerol, and 10% beta-mercaptoethanol) and denatured at 95°C for 10 min before being
615 storing at −80°C. Protein samples (20 µg per lane) were resolved and transferred to
616 nitrocellulose membranes (Bio-Rad). Total protein was measured using Revert 700 total
617 protein stain (926-11010, LI-COR), and membranes were blocked in Intercept (TBS) blocking
618 buffer (927-60001, LI-COR) for 1 hour at room temperature. Rabbit anti-PAX6 primary
619 antibody (901301; BioLegend; 1:500) was incubated at 4°C overnight. Secondary antibodies
620 [IRDye 800CW donkey anti-rabbit IgG secondary antibody (926-32213, LI-COR); 1:10,000]
621 were incubated for 1 hour at room temperature before data were captured on a LI-COR
622 Odyssey Classic. Western blots were replicated multiple times using 3 to 6 biological replicates
623 (organoids) per genotype. Data were analyzed using Image Studio Lite (LI-COR) and Microsoft
624 Excel.
625
626 *3D modelling*
627 Every 16th section of individual organoids labelled with TBR2 and DLX2 was sampled using
628 Zeiss Axio Scan Z1 slide scanner. A 200 x 200 µm grid was superimposed on each section and
629 fluorescent intensities corresponding to both DLX2 and TBR2 expression were measured for
630 each square. Expression data was then voxelised by assigning three-dimensional coordinates

631 to each grid square. Voxels were processed using the 3D modelling package Plotly (Sievert,
632 2020) to produce 3D heatmaps of TBR2 and DLX2 expression in each organoid. To determine
633 whether excitatory and inhibitory cells were mixed or segregated, voxels of TBR2 and DLX2
634 expression were used to calculate a EI value, given by the formula: log TBR2/DLX2 intensities
635 (Fig. 3B). This gave a value range to allow plotting 'excitatory' areas, which contain excitatory
636 neurons and 'inhibitory' areas where inhibitory neurons are enriched.
637
638 *Organoid dissociation and library preparation for single cell RNA sequencing*
639 Four organoids of each genotype from four separate differentiation batches were submitted
640 for scRNAseq. Briefly, each organoid were cut into smaller pieces with a scalpel and incubated
641 at 37°C in papain solution (Worthington) for 30 minutes (Velasco et al., 2019) before single
642 cell resuspension for downstream processing using 10X Genomics Chromium Next GEM Single
643 Cell 3' Reagent Kits v3.1 as per manufacturer's instruction. No organoids were pooled.
644 Sequencing was performed using Ilumina NovaSeq.
645
646 *PTN treatment*
647 Treatment on organoids were done according to (Notaras et al., 2022) with slight adjustments.
648 Briefly, organoids were treated with 50 ng/ml recombinant human PTN, reconstituted in
649 distilled water or water as control and added to differentiation media for 7 days starting from
650 day 13. The media was changed on days 13 and 14, and then every other day until they were
651 harvested on day 20. Number of organoids of each genotype ≥ 3 were used from ≥ 3
652 differentiation batches.
653
654 *Preprocessing of Single-Cell Transcriptomics Data*
655 Raw sequencing reads were aligned to the human reference genome (GRCh38, version 2024-
656 A) using Cell Ranger (v8.0.1, 10x Genomics), and cell-by-gene expression matrices were
657 generated. Ambient RNA contamination was removed using CellBender (v0.3.0), and potential
658 doublets were identified and excluded using scDblFinder (v1.18.0). Genes expressed in fewer
659 than 10 cells were excluded from downstream analyses. Only high-quality cells were retained
660 based on stringent quality control criteria: cells with mitochondrial RNA content below 10%,
661 ribosomal RNA content below 15%, hemoglobin RNA content below 5%, and between 500
662 and 10,000 detected genes were included. To further refine the dataset, Median Absolute

Deviation (MAD) filtering was applied to several quality metrics, including total Unique Molecular Identifier (UMI) counts, number of detected genes, mitochondrial and ribosomal RNA content, and the proportion of reads mapping to the top 20 most highly expressed genes. For each metric, the median and MAD were calculated across all cells, and cells exceeding five MADs from the median in any category were classified as outliers and removed. Stressed cells were also excluded using the Gruffi package. Additionally, cells not expressing FOXG1 were filtered out to focus our analysis on telencephalic cells.

Integration and Annotation of Single-Cell Transcriptomics Data

Data integration and batch correction were performed using scVI (scvi-tools v1.3.1.post1), which generated a unified latent representation from the combined datasets. Cell type prediction was performed using CellTypist, incorporating both its built-in "developmental brain" model (Braun et al., 2023) and custom models built from published datasets (He et al., 2024; Uzquiano et al., 2022; Wang et al., 2025a). Predicted cell labels were validated by cross-referencing with known marker genes.

Differential Expression Analysis

Pairwise comparisons between all cell type pairs were conducted using the Wilcoxon rank-sum test as implemented in Scanpy.

Pseudo-time and Bifurcation Analysis

Pseudotime calculation, cell developmental trajectory and branching were analysed using scFates (Faure et al., 2023).

Mouse Data Integration

Mouse single-cell data from (Manuel et al., 2022) were integrated with our dataset using scVI for cross-species comparison.

Whole Genome Analysis

Sequencing reads were quality-checked with FastQC (v0.12.1) and aligned to the human reference genome (GRCh38) using BWA-MEM (v0.7.18). BAM files were sorted, duplicates marked, and base quality scores recalibrated using GATK tools (version 4.6.1.0). Variants were

called per sample using GATK HaplotypeCaller in GVCF mode, followed by joint genotyping with CombineGVCFs and GenotypeGVCFs. Variant calls were filtered using GATK VariantFiltration and functionally annotated with the Ensembl Variant Effect Predictor (VEP, version 113.0).

Statistical analysis

For each between-organoid comparison (*PAX6*$^{+/+}$ vs *PAX6*$^{-/-}$), an ANOVA with nested mixed effects was performed, accounting for the random effect of batches and clones on variance in a hierarchical manner. Specifically, p-values and confidence intervals were calculated using a Type III Analysis of Variance with Satterthwaite's method.

Data availability

Raw sequences for both scRNAseq and WGS were deposited in ENA (PRJEB63603).

Code availability

All code used for data analysis in this article is available at Github (https://github.com/chan-ed/pax6_hom)

Acknowledgements

We thank Tilo Kunath for sharing the NAS2 hIPSC line. We are grateful to Spasimir Shishinyov, Alexander Markov, and Kanrayat Benjasupawan for assisting with organoid characterisation and troubleshooting, Thomas Theil and Thomas Pratt for helpful comments on the manuscript. This work was supported by Simons Initiative for the Developing Brain (grant number 529085, JOM and DJP) and the Medical Research Council (grant number MR/Y004299/1, WKC, JOM and DJP).

References

Anderson, S. A., Eisenstat, D. D., Shi, L. and Rubenstein, J. L. R. (1997). Interneuron Migration from Basal Forebrain to Neocortex: Dependence on Dlx Genes. *Science* **278**, 474–476.

Anderson, S. A., Marín, O., Horn, C., Jennings, K. and Rubenstein, J. L. R. (2001). Distinct cortical migrations from the medial and lateral ganglionic eminences. *Development* **128**, 353–363.

Bhaduri, A., Andrews, M. G., Leon, W. M., Jung, D., Shin, D., Allen, D., Jung, D., Schmunk, G., Haeussler, M., Salma, J., et al. (2020). Cell stress in cortical organoids impairs molecular subtype specification. *Nature* **578**, 142–148.

Birey, F., Andersen, J., Makinson, C. D., Islam, S., Wei, W., Huber, N., Fan, H. C., Metzler, K. R. C., Panagiotakos, G., Thom, N., et al. (2017). Assembly of functionally integrated human forebrain spheroids. *Nature* **545**, 54–59.

Braun, E., Danan-Gotthold, M., Borm, L. E., Lee, K. W., Vinsland, E., Lönnerberg, P., Hu, L., Li, X., He, X., Andrusivová, Ž., et al. (2023). Comprehensive cell atlas of the first-trimester developing human brain. *Science* **382**, eadf1226.

Bruining, H., Hardstone, R., Juarez-Martinez, E. L., Sprengers, J., Avramiea, A.-E., Simpraga, S., Houtman, S. J., Poil, S.-S., Dallares, E., Palva, S., et al. (2020). Measurement of excitation-inhibition ratio in autism spectrum disorder using critical brain dynamics. *Sci Rep* **10**, 9195.

Cadwell, C. R., Bhaduri, A., Mostajo-Radji, M. A., Keefe, M. G. and Nowakowski, T. J. (2019). Development and Arealization of the Cerebral Cortex. *Neuron* **103**, 980–1004.

Cederquist, G. Y., Asciolla, J. J., Tchieu, J., Walsh, R. M., Cornacchia, D., Resh, M. D. and Studer, L. (2019). Specification of positional identity in forebrain organoids. *Nature biotechnology* **37**, 436–444.

Chambers, S. M., Fasano, C. A., Papapetrou, E. P., Tomishima, M., Sadelain, M. and Studer, L. (2009). Highly efficient neural conversion of human ES and iPS cells by dual inhibition of SMAD signaling. *Nature biotechnology* **27**, 275–280.

Chang, Y., Berenson, J. R., Wang, Z. and Deuel, T. F. (2006). Dominant negative pleiotrophin induces tetraploidy and aneuploidy in U87MG human glioblastoma cells. *Biochemical and Biophysical Research Communications* **351**, 336–339.

Chen, X., Hartman, A. and Guo, S. (2015). Choosing Cell Fate Through a Dynamic Cell Cycle. *Curr Stem Cell Rep* **1**, 129–138.

Chung, C., Yang, X., Hevner, R. F., Kennedy, K., Vong, K. I., Liu, Y., Patel, A., Nedunuri, R., Barton, S. T., Noel, G., et al. (2024). Cell-type-resolved mosaicism reveals clonal dynamics of the human forebrain. *Nature* **629**, 384–392.

D'Antonio, M., Benaglio, P., Jakubosky, D., Greenwald, W. W., Matsui, H., Donovan, M. K. R., Li, H., Smith, E. N., D'Antonio-Chronowska, A. and Frazer, K. A. (2018). Insights into the mutational burden of human induced pluripotent stem cells from an integrative omics approach. *Cell Rep* **24**, 883–894.

Delgado, R. N., Allen, D. E., Keefe, M. G., Mancia Leon, W. R., Ziffra, R. S., Crouch, E. E., Alvarez-Buylla, A. and Nowakowski, T. J. (2022). Individual human cortical progenitors can produce excitatory and inhibitory neurons. *Nature* **601**, 397–403.

Devine, M. J., Ryten, M., Vodicka, P., Thomson, A. J., Burdon, T., Houlden, H., Cavaleri, F., Nagano, M., Drummond, N. J., Taanman, J.-W. W., et al. (2011). Parkinson's disease induced pluripotent stem cells with triplication of the α-synuclein locus. *Nature Communications* **2**, 440.

Domínguez Conde, C., Xu, C., Jarvis, L. B., Rainbow, D. B., Wells, S. B., Gomes, T., Howlett, S. K., Suchanek, O., Polanski, K., King, H. W., et al. (2022). Cross-tissue immune cell analysis reveals tissue-specific features in humans. *Science* **376**, eabl5197.

Engelkamp, D., Rashbass, P., Seawright, A. and Heyningen, V. van (1999). Role of Pax6 in development of the cerebellar system. *Development* **126**, 3585–3596.

Eze, U. C., Bhaduri, A., Haeussler, M., Nowakowski, T. J. and Kriegstein, A. R. (2021). Single-cell atlas of early human brain development highlights heterogeneity of human neuroepithelial cells and early radial glia. *Nat Neurosci* **24**, 584–594.

Faure, L., Soldatov, R., Kharchenko, P. V. and Adameyko, I. (2023). scFates: a scalable python package for advanced pseudotime and bifurcation analysis from single-cell data. *Bioinformatics* **39**, btac746.

Garcia-Gutierrez, P., Juarez-Vicente, F., Wolgemuth, D. J. and Garcia-Dominguez, M. (2014). Pleiotrophin antagonizes Brd2 during neuronal differentiation. *J Cell Sci* **127**, 2554–2564.

Glaser, T., Jepeal, L., Edwards, J. G., Young, S. R., Favor, J. and Maas, R. L. (1994). PAX6 gene dosage effect in a family with congenital cataracts, aniridia, anophthalmia and central nervous system defects. *Nat Genet* **7**, 463–471.

Gomes, A. R., Fernandes, T. G., Vaz, S. H., Silva, T. P., Bekman, E. P., Xapelli, S., Duarte, S., Ghazvini, M., Gribnau, J., Muotri, A. R., et al. (2020). Modeling Rett Syndrome With Human Patient-Specific Forebrain Organoids. *Frontiers in Cell and Developmental Biology* **8**,.

González-Castillo, C., Ortuño-Sahagún, D., Guzmán-Brambila, C., Pallàs, M. and Rojas-Mayorquín, A. E. (2015). Pleiotrophin as a central nervous system neuromodulator, evidences from the hippocampus. *Front. Cell. Neurosci.* **8**,.

Gorski, J. A., Talley, T., Qiu, M., Puelles, L., Rubenstein, J. L. R. and Jones, K. R. (2002). Cortical Excitatory Neurons and Glia, But Not GABAergic Neurons, Are Produced in the Emx1-Expressing Lineage. *J. Neurosci.* **22**, 6309–6314.

Guo, T., Liu, G., Du, H., Wen, Y., Wei, S., Li, Z., Tao, G., Shang, Z., Song, X., Zhang, Z., et al. (2019). Dlx1/2 are Central and Essential Components in the Transcriptional Code for Generating Olfactory Bulb Interneurons. *Cereb Cortex* **29**, 4831–4849.

Hansen, D. V., Lui, J. H., Parker, P. R. L. and Kriegstein, A. R. (2010). Neurogenic radial glia in the outer subventricular zone of human neocortex. *Nature* **464**, 554–561.

Haubst, N., Berger, J., Radjendirane, V., Graw, J., Favor, J., Saunders, G. F., Stoykova, A. and Götz, M. (2004). Molecular dissection of Pax6 function: The specific roles of the paired domain and homeodomain in brain development. *Development* **131**, 6131–6140.

He, Z., Dony, L., Fleck, J. S., Szałata, A., Li, K. X., Slišković, I., Lin, H.-C., Santel, M., Atamian, A., Quadrato, G., et al. (2024). An integrated transcriptomic cell atlas of human neural organoids. *Nature* **635**, 690–698.

Keefe, M. G., Steyert, M. R. and Nowakowski, T. J. (2025). Lineage-resolved atlas of the developing human cortex. *Nature* **647**, 194–202.

Kerwin, J., Yang, Y., Merchan, P., Sarma, S., Thompson, J., Wang, X., Sandoval, J., Puelles, L., Baldock, R. and Lindsay, S. (2010). The HUDSEN Atlas: a three-dimensional (3D) spatial framework for studying gene expression in the developing human brain. *Journal of Anatomy* **217**, 289–299.

Kroll, T. T. and O'Leary, D. D. M. (2005). Ventralized dorsal telencephalic progenitors in Pax6 mutant mice generate GABA interneurons of a lateral ganglionic eminence fate. *Proceedings of the National Academy of Sciences of the United States of America* **102**, 7374–7379.

Lancaster, M. A., Renner, M., Martin, C.-A. A., Wenzel, D., Bicknell, L. S., Hurles, M. E., Homfray, T., Penninger, J. M., Jackson, A. P. and Knoblich, J. A. (2013). Cerebral organoids model human brain development and microcephaly. *Nature* **501**, 373-+.

Li, H., Xu, L., Jiang, W., Qiu, X., Xu, H., Zhu, F., Hu, Y., Liang, S., Cai, C., Qiu, W., et al. (2023). Pleiotrophin ameliorates age-induced adult hippocampal neurogenesis decline and cognitive dysfunction. *Cell Reports* **42**, 113022.

Lindsay, S., Sarma, S., Martínez-de-la-Torre, M., Kerwin, J., Scott, M., Luis Ferran, J., Baldock, R. and Puelles, L. (2005). Anatomical and gene expression mapping of the ventral pallium in a three-dimensional model of developing human brain. *Neuroscience* **136**, 625–632.

Manuel, M. N., Mi, D., Mason, J. O. and Price, D. J. (2015). Regulation of cerebral cortical neurogenesis by the Pax6 transcription factor. *Frontiers in Cellular Neuroscience* **9**,.

Manuel, M., Tan, K. B., Kozic, Z., Molinek, M., Marcos, T. S., Razak, M. F. A., Dobolyi, D., Dobie, R., Henderson, B. E. P., Henderson, N. C., et al. (2022). Pax6 limits the competence of developing cerebral cortical cells to respond to inductive intercellular signals. *PLOS Biology* **20**, e3001563.

Meng, K., Rodríguez-Peña, A., Dimitrov, T., Chen, W., Yamin, M., Noda, M. and Deuel, T. F. (2000). Pleiotrophin signals increased tyrosine phosphorylation of β-catenin through inactivation of the intrinsic catalytic activity of the receptor-type protein tyrosine phosphatase β/ζ. *Proceedings of the National Academy of Sciences* **97**, 2603–2608.

Mo, Z. and Zecevic, N. (2008). Is Pax6 Critical for Neurogenesis in the Human Fetal Brain? *Cereb Cortex* **18**, 1455–1465.

Notaras, M., Lodhi, A., Dündar, F., Collier, P., Sayles, N. M., Tilgner, H., Greening, D. and Colak, D. (2022). Schizophrenia is defined by cell-specific neuropathology and multiple neurodevelopmental mechanisms in patient-derived cerebral organoids. *Mol Psychiatry* **27**, 1416–1434.

Nowakowski, T. J., Bhaduri, A., Pollen, A. A., Alvarado, B., Mostajo-Radji, M. A., Di Lullo, E., Haeussler, M., Sandoval-Espinosa, C., Liu, S. J., Velmeshev, D., et al. (2017). Spatiotemporal gene expression trajectories reveal developmental hierarchies of the human cortex. *Science (New York, N.Y.)* **358**, 1318–1323.

Ochi, S., Manabe, S., Kikkawa, T. and Osumi, N. (2022). Thirty Years' History since the Discovery of Pax6: From Central Nervous System Development to Neurodevelopmental Disorders. *Int J Mol Sci* **23**, 6115.

Osaki, T., Duenki, T., Chow, S. Y. A., Ikegami, Y., Beaubois, R., Levi, T., Nakagawa-Tamagawa, N., Hirano, Y. and Ikeuchi, Y. (2024). Complex activity and short-term plasticity of human cerebral organoids reciprocally connected with axons. *Nat Commun* **15**, 2945.

Pollen, A. A., Nowakowski, T. J., Chen, J., Retallack, H., Sandoval-Espinosa, C., Nicholas, C. R., Shuga, J., Liu, S. J., Oldham, M. C., Diaz, A., et al. (2015). Molecular Identity of Human Outer Radial Glia during Cortical Development. *Cell* **163**, 55–67.

Reillo, I., de Juan Romero, C., García-Cabezas, M. Á. and Borrell, V. (2011). A role for intermediate radial glia in the tangential expansion of the mammalian cerebral cortex. *Cereb Cortex* **21**, 1674–1694.

Schmidt-Sidor, B., Szymańska, K., Williamson, K., van Heyningen, V., Roszkowski, T., Wierzba-Bobrowicz, T. and Zaremba, J. (2009). Malformations of the brain in two fetuses with a compound heterozygosity for two PAX6 mutations. *Folia Neuropathol* **47**, 372–382.

Sharf, T., Van Der Molen, T., Glasauer, S. M. K., Guzman, E., Buccino, A. P., Luna, G., Cheng, Z., Audouard, M., Ranasinghe, K. G., Kudo, K., et al. (2022). Functional neuronal circuitry and oscillatory dynamics in human brain organoids. *Nat Commun* **13**, 4403.

Shi, Y., Ping, Y.-F., Zhou, W., He, Z.-C., Chen, C., Bian, B.-S.-J., Zhang, L., Chen, L., Lan, X., Zhang, X.-C., et al. (2017). Tumour-associated macrophages secrete pleiotrophin to promote PTPRZ1 signalling in glioblastoma stem cells for tumour growth. *Nat Commun* **8**, 15080.

Shi, Y., Wang, M., Mi, D., Lu, T., Wang, B., Dong, H., Zhong, S., Chen, Y., Sun, L., Zhou, X., et al. (2021). Mouse and human share conserved transcriptional programs for interneuron development. *Science (New York, N.Y.)* **374**, eabj6641.

Sievert, C. (2020). *Interactive Web-Based Data Visualization with R, plotly, and shiny*. Boca Raton: Chapman and Hall/CRC.

Solomon, B. D., Pineda-Alvarez, D. E., Balog, J. Z., Hadley, D., Gropman, A. L., Nandagopal, R., Han, J. C., Hahn, J. S., Blain, D., Brooks, B., et al. (2009). Compound heterozygosity for mutations in PAX6 in a patient with complex brain anomaly, neonatal diabetes mellitus, and microophthalmia. *American Journal of Medical Genetics, Part A* **149**, 2543–2546.

Tang, C., Wang, M., Wang, P., Wang, L., Wu, Q. and Guo, W. (2019). Neural Stem Cells Behave as a Functional Niche for the Maturation of Newborn Neurons through the Secretion of PTN. *Neuron* **101**, 32-44.e6.

Tapp, H., Hernandez, D. J., Neame, P. J. and Koob, T. J. (1999). Pleiotrophin inhibits chondrocyte proliferation and stimulates proteoglycan synthesis in mature bovine cartilage. *Matrix Biology* **18**, 543–556.

Tzoulaki, I., White, I. M. and Hanson, I. M. (2005). PAX6 mutations: genotype-phenotype correlations. *BMC Genet* **6**, 27.

Uzquiano, A., Kedaigle, A. J., Pigoni, M., Paulsen, B., Adiconis, X., Kim, K., Faits, T., Nagaraja, S., Antón-Bolaños, N., Gerhardinger, C., et al. (2022). Proper acquisition of cell class identity in organoids allows definition of fate specification programs of the human cerebral cortex. *Cell* **185**, 3770-3788.e27.

Velasco, S., Kedaigle, A. J., Simmons, S. K., Nash, A., Rocha, M., Quadrato, G., Paulsen, B., Nguyen, L., Adiconis, X., Regev, A., et al. (2019). Individual brain organoids reproducibly form cell diversity of the human cerebral cortex. *Nature* **570**, 523–527.

Vértesy, Á., Eichmüller, O. L., Naas, J., Novatchkova, M., Esk, C., Balmaña, M., Ladstaetter, S., Bock, C., von Haeseler, A. and Knoblich, J. A. (2022). Gruffi: an algorithm for computational removal of stressed cells from brain organoid transcriptomic datasets. *The EMBO Journal* **41**, e111118.

Walcher, T., Xie, Q., Sun, J., Irmler, M., Beckers, J., Öztürk, T., Niessing, D., Stoykova, A., Cvekl, A., Ninkovic, J., et al. (2013). Functional dissection of the paired domain of Pax6 reveals molecular mechanisms of coordinating neurogenesis and proliferation. *Development (Cambridge)* **140**, 1123–1136.

Wang, X. (2020). Chapter Three - Pleiotrophin: Activity and mechanism. In *Advances in Clinical Chemistry* (ed. Makowski, G. S.), pp. 51–89. Elsevier.

Wang, L., Wang, C., Moriano, J. A., Chen, S., Zuo, G., Cebrián-Silla, A., Zhang, S., Mukhtar, T., Wang, S., Song, M., et al. (2025a). Molecular and cellular dynamics of the developing human neocortex. *Nature* 1–10.

Wang, L., Wang, C., Moriano, J. A., Chen, S., Zuo, G., Cebrián-Silla, A., Zhang, S., Mukhtar, T., Wang, S., Song, M., et al. (2025b). Molecular and cellular dynamics of the developing human neocortex. *Nature* 1–10.

Xu, H. E., Rould, M. A., Xu, W., Epstein, J. A., Maas, R. L. and Pabo, C. O. (1999). Crystal structure of the human Pax6 paired domain–DNA complex reveals specific roles for the linker region and carboxy-terminal subdomain in DNA binding. *Genes Dev* **13**, 1263–1275.

Yanagisawa, H., Komuta, Y., Kawano, H., Toyoda, M. and Sango, K. (2010). Pleiotrophin induces neurite outgrowth and up-regulates growth-associated protein (GAP)-43 mRNA through the ALK/GSK3β/β-catenin signaling in developing mouse neurons. *Neuroscience Research* **66**, 111–116.

Yu, Y., Zeng, Z., Xie, D., Chen, R., Sha, Y., Huang, S., Cai, W., Chen, W., Li, W., Ke, R., et al. (2021). Interneuron origin and molecular diversity in the human fetal brain. *Nature Neuroscience* **24**, 1745–1756.